Monthly Notices of the ROYAL ASTRONOMICAL SOCIETY
MNRAS **507,** 2825–2842 (2021) https://doi.org/10.1093/mnras/stab2398
Advance Access publication 2021 August 20

A holistic review of a galactic interaction

Douglas Grion Filho,[1★] Kathryn V. Johnston,[1,2] Eloisa Poggio,[3,4] Chervin F. P. Laporte,[5,6,7,4] Ronald Drimmel[3] and Elena D'Onghia[8]

[1]*Department of Astronomy, Columbia University, 550 West 120th Street, New York, NY 10027, USA*
[2]*Center for Computational Astrophysics, Flatiron Institute, 162 5th Av., New York City, NY 10010, USA*
[3]*Osservatorio Astrofisico di Torino, Istituto Nazionale di Astrofisica (INAF), I-10025 Pino Torinese, Italy*
[4]*Université Côte d'Azur, Observatoire de la Côte d'Azur, CNRS, Laboratoire Lagrange, 06108, France*
[5]*Institut de Ciències del Cosmos (ICCUB), Universitat de Barcelona (IEEC-UB), Martí i Franquès 1, E-08028 Barcelona, Spain*
[6]*Kavli Institute for the Physics and Mathematics of the Universe (WPI), The University of Tokyo Institutes for Advanced Study (UTIAS) The University of Tokyo, Chiba 277-8583, Japan*
[7]*Department of Physics & Astronomy, University of Victoria, 3800 Finnerty Road, Victoria BC, V8P 5C2 Canada*
[8]*University of Wisconsin, Madison, Astronomy Department, 475 N Charter Str, Wisconsin 53706, USA*

Accepted 2021 August 16. Received 2021 July 29; in original form 2020 December 14

ABSTRACT

Our situation as occupants of the Milky Way (MW) Galaxy, bombarded by the Sagittarius dwarf galaxy, provides an intimate view of physical processes that can lead to the dynamical heating of a galactic disc. While this evolution is instigated by Sagittarius, it is also driven by the intertwined influences of the dark matter halo and the disc itself. We analyse an *N*-body simulation following a Sagittarius-like galaxy interacting with a MW-like host to disentangle these different influences during the stages of a minor merger. The accelerations in the disc plane from each component are calculated for each snapshot in the simulation, and then decomposed into Fourier series on annuli. The analysis maps quantify and compare the scales of the individual contributions over space and through time: (i) accelerations due to the satellite are only important around disc passages; (ii) the influence around these passages is enhanced and extended by the distortion of the dark matter halo; (iii) the interaction drives disc asymmetries within and perpendicular to the plane and the self-gravity of these distortions increase in importance with time eventually leading to the formation of a bar. These results have interesting implications for identifying different influences within our own Galaxy. Currently, Sagittarius is close enough to a plane crossing to search for localized signatures of its effect at intermediate radii, the distortion of the MW's dark matter halo should leave its imprint in the outer disc and the disc's own self-consistent response is sculpting the intermediate and inner disc.

Key words: Galaxy: disc – Galaxy: evolution – Galaxy: kinematics and dynamics – Galaxy: structure – Local Group.

1 INTRODUCTION

Recently, there has been a significant revision in our perception of the Milky Way (hereafter MW), shifting from an equilibrium picture to one rife with signatures of disequilibrium, as revealed by large-scale stellar surveys.

North/South asymmetries in density and velocity structure were found in the Galactic disc using data from SDSS Widrow et al. (2012) and Williams et al. (2013). Analysis of LAMOST and RAVE suggested these local asymmetries to be part of a large-scale vertical wave (Carlin et al. 2013; Xu et al. 2015). Studies motivated by observations of M-giants selected using 2MASS photometry showed this wave to be propagating from the Solar Neighborhood to the outer disc (Price-Whelan et al. 2015; Li et al. 2017; Bergemann et al. 2018; Sheffield et al. 2018). In addition to this, the disc of our Galaxy presents a large-scale warp (Burke 1957; Kerr 1957; Djorgovski & Sosin 1989; López-Corredoira et al. 2002; Reylé et al. 2009; Amôres, Robin & Reylé 2017; Chen et al. 2019; Skowron et al. 2019), suggesting that the MW might be responding to external/internal torques and perturbations. Indeed, the initial discovery of disc asymmetries in SDSS led Widrow et al. (2014) to investigate the nature of 'bending' and 'breathing' modes in galactic discs (see Dubinski & Kuijken 1995, for an early discussion of bending modes) and there have been several studies of their appearance in *N*-body and cosmological hydrodynamical simulations of interactions between satellite and parent galaxies (Gómez et al. 2013; D'Onghia et al. 2016; Gómez et al. 2017; Laporte et al. 2018a). The second data release from the *Gaia* mission (hereafter *Gaia* DR2) connected the disparate lines of evidence from prior surveys with a global view that mapped these ripples in the disc on a 'macroscopic' scale (Gaia Collaboration 2018a; Friske & Schönrich 2019) in both vertical and radial directions (Antoja et al. 2018). Vertical motions also suggest that the Galactic warp might be evolving with time (Poggio et al. 2020b; Cheng et al. 2020). The 'microscopic' counterpart of the ripples was revealed by *Gaia* DR2 in the form of spirals in the vertical component of phase-space (e.g. in density the z-v_z plane) – a signature of incomplete phase-mixing following a disturbance (Antoja et al. 2018; Binney & Schönrich 2018; Laporte et al. 2019; Bland-Hawthorn et al. 2019).

★ E-mail: df2629@columbia.edu

In the plane of the disc, several kinematic ridges in the $U-V$ velocity plane have been revealed in the Solar neighborhood (Gaia Collaboration 2018b; Ramos, Antoja & Figueras 2018). Other ridges have also been shown in the (R, v_T) plane (Antoja et al. 2018; Kawata et al. 2018; Laporte et al. 2020) and in action space (Trick, Coronado & Rix 2019). Furthermore, Gaia Collaboration (2018b), Friske & Schönrich (2019), and Eilers et al. (2020) have shown both local and global spiral waves in mean galactocentric radial velocities. Several dynamical processes could explain their origin, such as spiral arms (Quillen 2003; Quillen & Minchev 2005; Hunt et al. 2019; Sellwood et al. 2019; Khoperskov et al. 2020), bar resonances (Fragkoudi et al. 2019, 2020; Hunt et al. 2019; Monari et al. 2019; Kawata et al. 2020; Laporte et al. 2020; Trick et al. 2021), or the response of the disc to an infalling satellite (Minchev et al. 2009; Gómez et al. 2012; Antoja et al. 2018; Khanna et al. 2019; Laporte et al. 2019).

Possible culprits for causing vertical and in-plane disturbances are the satellite galaxies that orbit the MW. (Note that Khoperskov et al. (2019) pointed to buckling bar as another plausible explanation for vertical disturbances.) Parent/satellite galaxy interactions enjoy a rich literature around the topics of dynamical friction, satellite disruption, and disc response (Johnston, Spergel & Hernquist 1995; Walker, Mihos & Hernquist 1996). Much of this past work has concentrated on the long-term and orbit-averaged effect of dynamical heating of discs, and the implications for galaxy evolution (Toth & Ostriker 1992; Velazquez & White 1999). In contrast, the detail of the current MW data sets instead offers the opportunity to study the mechanisms of disc heating in process.

Past work has also emphasized and explored the importance of all galactic components – disc, satellite, and dark matter halo (hereafter DM halo) – in driving dynamical evolution through mutual gravitational interactions (Weinberg 1998, 1999; Vesperini & Weinberg 2001; Weinberg & Blitz 2006; Gómez et al. 2016; Laporte et al. 2018a,b; Garavito-Camargo et al. 2020): the satellite deforms the DM halo; the deformation of the DM halo both affects the orbit of the satellite and can in turn perturb the disc; the perturbation of the disc can drag on both the satellite and the DM halo; and the satellite can directly affect the disc during pericenters and plane crossings. Recently, Laporte et al. (2018b) used N-body simulations to demonstrate that the interaction of the MW with its closest satellite companion, the Sagittarius dwarf galaxy (herefter Sgr), could plausibly produce many of the disc disturbances that had been noted prior to *Gaia* DR2, both on large scales and small scales. They confirmed the two-phase seeding mechanism for the disc response through the action of torques from the dark matter halo wake later transitioning to tides from Sgr itself. These same models were subsequently found to contain similar scales in the detailed phase-structure in the *Gaia* data set in multiple dimensions (Laporte et al. 2019). Subsequent work (Bland-Hawthorn & Tepper-Garcia 2020; Hunt et al. 2021) connects these features with even higher resolution simulations.

This paper characterizes the complex dynamical interaction between the MW's disc, DM halo, and Sgr. Our aim is to retrieve what spatial and temporal regimes in the disc response can be attributed to the influence of each source of perturbation. To this end, we work with one specific model from the series of N-body simulations developed in Laporte et al. (2018b) that best reflects the scale of the response seen in the MW. Our paper is a companion to the analysis of Poggio et al. (2020a), who used Fourier Series to interpret the vertical evolution of the disc in this same simulation (see also Chequers & Widrow 2017; Chequers, Widrow & Darling 2018; Laporte et al. 2018b, for prior work also using Fourier decomposition to study disc evolution). We add to this study by first looking at Fourier Series of the response of the disc in density as a Fourier series over time at each radius. We subsequently decompose the *acceleration* due to each component (disc, DM halo, and Sgr) in the disc plane. This approach allows us to compare amplitude, spatial scales, and time-scales of these different influences and connect responses to their origin as a natural follow-up to (Laporte et al. 2018b).

The paper is structured as follows: Section 2 goes over the simulations and numerical methods used in this work; Section 3 explores the context for our study of influences by first reviewing the evolving properties of Sgr and the disc's density structure; Section 4 shows the results of our Fourier analysis of drivers of disc evolution; and Section 5 summarizes our results and presents our conclusions.

2 NUMERICAL METHODS

2.1 Simulation description

The simulation used in this work is taken from Laporte et al. (2018b), which report on a series of live N-body simulations of the interaction between a Sgr-like galaxy with a MW-like host. The work contains several different models, some of them also taking into account the effects of the Large Magellanic Cloud (LMC) on a first infall orbit. In this work, however, we focus on the L2 model of Laporte et al. (2018b), which looks only at the interaction with Sgr alone. We choose the L2 model because other more massive progenitor models produced disc responses with amplitude in excess of what is observed (see discussion in Laporte et al. 2019). Unlike prior models, the simulation follows the response of the Galaxy since the time of first crossing of the virial radius to the present-day, which was central to depict and characterize the early influence of the dark matter halo wake (see also Weinberg 1998; Vesperini & Weinberg 2001; Gómez et al. 2016) excited by Sgr on the disc during the course of its evolution since z 1.

The N-body simulation presented here ran with the tree-code *GADGET* $-$ 3. The simulated MW had the following properties: a spherical Dark Matter Halo following a Hernquist profile (Hernquist 1990) with mass $M_h = 10^{12}$ M$_\odot$ and a scale length $a_h = 52$ kpc, an exponential disc of $M_{\rm disc} = 6 \times 10^{10}$ M$_\odot$, with a scale length of $R_d = 3.5$ kpc, scale height of $h_d = 0.53$ kpc, and a central bulge represented by a Hernquist Sphere with mass of $M_{\rm bulge} = 10^{10}$ M$_\odot$ and scale length $a = 0.7$ kpc. The DM halo is adiabatically contracted leading to a final circular velocity of $V_{\rm circ} = 239$ km s^{-1} at $R_0 = 8$ kpc as shown by Fig. 1.

Sgr's dark matter halo in these simulations is parametrized using a Hernquist profile with varying masses and scale lengths depending on the model. For the model we are using in this analysis – the L2 model – Sgr is given a virial mass model of $M_{200} = 6.0 \times 10^{10}$ M$_\odot$, and its Hernquist parameters are $M_h = 8.0 \times 10^{10}$ M$_\odot$ and $a_h = 8$ kpc. These parameters for Sgr are chosen to closely match their corresponding NFW haloes but with steeper fall-off at large radii. The stellar content matches the stellar-halo mass relation from abundance matching or galaxy formation models (Moster, Naab & White 2013; Sawala et al. 2016). The final dwarf properties are broadly consistent with recent observational work on the progenitor stellar mass and stream velocity dispersions (e.g. Niederste-Ostholt et al. 2010; Gibbons, Belokurov & Evans 2017).

The particle masses in the simulation are $m_h = 2.6 \times 10^4$ M$_\odot$, $m_d = 1.2 \times 10^4$ M$_\odot$, and $m_b = 10^4$ M$_\odot$ for the dark matter, disc, and bulge components, respectively. The softening lengths for the disc are $\epsilon_h = 60$ pc and $\epsilon_d = \epsilon_b = 30$ pc. The simulation represents the disc with 5 million particles and the DM halo with 40 million particles,

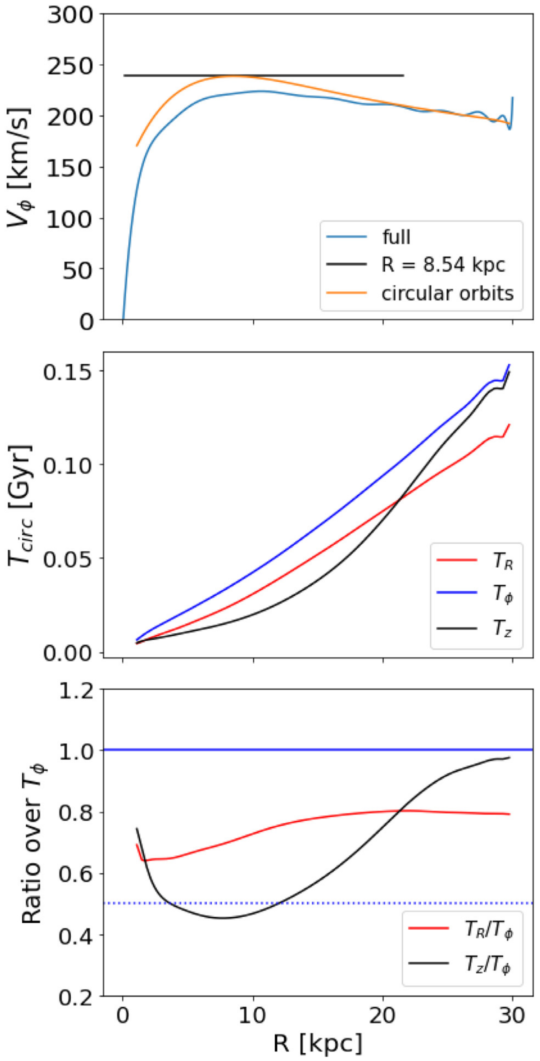

Figure 1. Rotation curve of the disc for the first snapshot (top). Orange line is the mean rotation curve for particles on roughly circular orbits, while the blue line is mean V_ϕ for all particles. The black line at $R = 8.54$ kpc indicates the point at which $\mathrm{d}V_{\mathrm{circ}}/\mathrm{d}t = 0$. The middle panel shows the periods associated with the three fundamental frequencies (κ, Ω, and ν, respectively) for particles on circular orbits. Finally, the bottom panel shows the ratio of these periods with respect to T_ϕ, with a dotted line at a ratio equal to 0.5 and a solid line at 1.0.

such as to minimize the effect of heating between the different species.

Our snapshot analyses are performed in a reference frame centered on the bulge and aligned with the galactic mid-plane, as outlined in Gómez et al. (2013) and Laporte et al. (2018b). This means that our analysis does not follow the re-orientation or motion of the disc relative to initial conditions, but instead looks at the net acceleration, the disc experiences relative to its own geometrical configuration.

2.2 Characterizing influences on the disc

For each snapshot in the simulation, we assess the influence that the different components have on the disc by binning the disc mid-plane in radius and azimuth using a 100 × 100 polar grid – i.e. dividing R into 100 slices ranging from 0 to 30 kpc, while also slicing ϕ into 100 slices from 0 to 2π. We then estimate the acceleration at each grid point, i due to each component (disc, DM halo, and Sgr) by simply summing over individual forces from each particle,

$$a_{q,i} = \sum_{j=0}^{N_{\mathrm{comp}}} -\frac{Gm_j}{(\mathrm{d}_{ij} + \alpha)^2 \mathrm{d}_{ij}} \times (q_i - q_j) \tag{1}$$

where d is the distance between the component particle and the $z = 0$ grid point, q is the coordinate (x, y, or z) and $\alpha = 0.7$ kpc is a softening parameter to lessen the effects of component particles that just so happen to lie in the $z = 0$ plane. Since we are interested in drivers of the evolution of the disc's structure rather than its overall motion, we assess the tidal accelerations from Sgr and the DM Halo by subtracting the acceleration at the discs center at each grid point.

We utilize Fourier Transforms in order to summarize both the response (in density) of and influences (by projecting our acceleration fields into cylindrical coordinates) on the disc. For a given ring at galactocentric radius R, we express deviations from initial conditions ΔQ in the quantity Q as an infinite sum of Fourier terms in Galactic azimuth ϕ:

$$\Delta Q(R, \phi) = A_0(R) + \sum_{m=1}^{\infty} A_m(R) \cos(m\phi - \phi_m(R)) \tag{2}$$

where $A_m(R)$ is the amplitude of the mth Fourier term and $\phi_m(R)$ is the phase. (Note that the only non-zero component in any case early in the simulation will be the radial acceleration, a_R, which is keeping the disc particles in orbit.) The azimuthal angle ϕ is taken as positive in the direction of Galactic rotation. Rings in R are chosen to contain the same number of particles, so they are narrower in the inner and wider in the outer disc.

3 RESULTS I: OVERVIEW OF THE INTERACTION AND RESPONSES

This section first reviews the *responses* to the intertwined gravitational interactions by summarizing the evolution in the simulation, in particular, for Sgr (Section 3.1) and the disc (Sections 3.2 and 4.1). We then go on to distinguish *drivers* of that evolution in Section 4.

3.1 Sagittarius' mass and orbit, interaction regimes and epochs, and the global mass profile

In this simulation, Sagittarius (Sgr) is the instigator of the evolution of the disc. Fig. 2, taken from Poggio et al. (2020a), shows the orbit of the satellite both in spherical radius, r and vertical position, z, along with an estimate for its instantaneous mass (described in Carr et al, in preparation). We can broadly split the simulation into into four 'epochs' in time.

(i) Epoch 0: Prior to the first impact, we can examine how the disc evolves in isolation. We will use the scale of Fourier amplitudes in this regime to understand the significance of those seen in all subsequent regimes. (see appendix C of Poggio et al. 2020a, which demonstrates that the nature of features seen in this regime are in common with those strictly in isolation.)

(ii) Epoch 1: Between impacts 1 and 2, interactions are far enough apart to allow the disc to relax between plane-crossings and we can study this secular, internal process.

(iii) Epoch 2: Impacts 2–5 cross the plane on time-scales comparable to the orbital time-scales in the middle disc so we might expect some resonant responses.

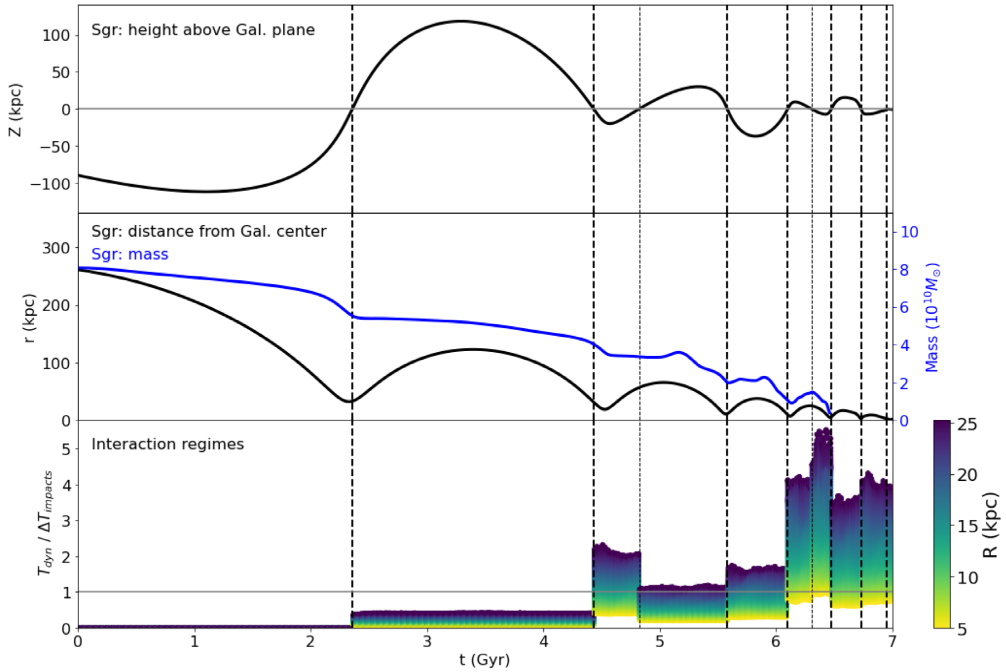

Figure 2. Interaction regimes (reproduced from fig. 1 of Poggio et al. (2020a)). Top panels show height above the Galactic plane (z, black line, upper panel), distance from the Galactic center in spherical coordinates (r, black line, middle panel) and mass loss as a function of time (blue line, middle panel) of the Sagittarius Dwarf Galaxy as a function of time. The mass-loss curve ends at the approximate 'present day' snapshot (6.4 Gyr). Vertical lines represent the times of disc crossings. The bottom panel demonstrates how the simulation can be broadly split into regimes by comparing the local orbital time $T_{\rm dyn}$ to the time between impacts $\Delta T_{\rm impact}$: in Regime 0, before the first impact, the disc evolves in isolation; in Regime 1, between impacts 1 and 2 where the effect of a single impact can be studied; in Regime 2, the disc is being impacted repeatedly on similar time-scales to an orbit; and in Regime 3, the impacts occur multiple times per orbit.

(iv) Epoch 3: For the remainder of the simulation, repeated impacts on short time-scales cause a strong and complicated response in the Galactic disc.

The bottom panel of Fig. 2 shows how different regions of the disc – e.g. inner (<5 kpc, yellow), middle (5–15 kpc, green), and outer (>15 kpc, blue) – are directly impacted in different ways during each epoch and expected to respond on different time-scales. Following Poggio et al. (2020a), we adopt four characteristic interaction 'Regimes' in space (which are time dependent, based on the ratio $T_{\rm dyn}/\Delta T_{\rm impacts}$, where $\Delta T_{\rm impacts}$ is the time interval between two impacts of Sgr and $T_{\rm dyn}$ is the local orbital time at cylindrical radius R in the disc plane ($\sim 2\pi R/V_\phi$, where V_ϕ is the mean azimuthal velocity).

(i) Regimes, 0, 1, 2, and 3 correspond to a ratio of $T_{\rm dyn}/\Delta T_{\rm impacts}$ of 0, less than unity, of order unity and greater than unity respectively, i.e. the disc evolving in isolation [0], or in response to: a single impact [1]; impacts repeated roughly every orbit [2], or multiple impacts per orbit [3].

Fig. 3 (top) gives a global view of the overall evolution by showing how the enclosed mass within a spherical radius $r - M(<r)$ – changes from the beginning (1 Gyr – solid lines) to the end of the simulation (6.95 Gyr – dashed lines) for each component in the simulation: Sgr (red), DM halo (black), and disc (blue). Note that this is also an indicator of changes to the net acceleration at each radius. The bottom panel of the figure shows the fractional change $\Delta M(<r)/M(r)$ relative to the initial DM halo distribution for each component. The figure demonstrates that the mass distribution of the DM halo does not significantly change throughout the simulation, though there is a small inward migration of mass into the disc regions. The disc experiences most change in its mass distribution within the inner disc ($r < 5$ kpc). Sgr's debris contributes a negligible fraction of these mass changes within the disc. The plot emphasizes that the overall mass redistribution, though measurable, is small (order per cent changes).

3.2 Disc density evolution

Fig. 4 gives a visual idea of the disc response by showing a sample snapshot of disc surface density in each Epoch (0–3 in sequence in left-to-right panels). Since there is a strong radial dependence for each spatial Regime (bottom of Fig. 2), some can co-exist at different radii within each panel. For example, the last panel of Fig. 4, showing the disc at time $t = 6.95$ Gyr contains Regimes 1, 2, and 3 depending on whether one is considering the inner, middle, or outer regions of the disc. In Epoch 0, the disc is stable and almost featureless, other than some low-level self-consistent 'ringing' left over from the initialization routine (see below for more discussion); in Epoch 1 the first impact drives the disc to form a regular two-armed spiral pattern; in Epoch 2, the repeated impacts on orbital times excite multiple overlapping spiral patterns; in Epoch 3, the impacts themselves are the dominant influence and the disc is sufficiently perturbed to form a bar.

Fig. 5 summarizes the evolution of the disc by presenting Fourier decompositions of deviations in the disc surface density, $\Delta\Sigma$, from its state at $t_0 = 1$ Gyr. This allows us to show a quantitative representation of the evolution throughout the entire simulation over space (i.e. radius on the y-axis) and for every snapshot in time (on the x-axis), with six numbers – i.e. the amplitudes and phases of

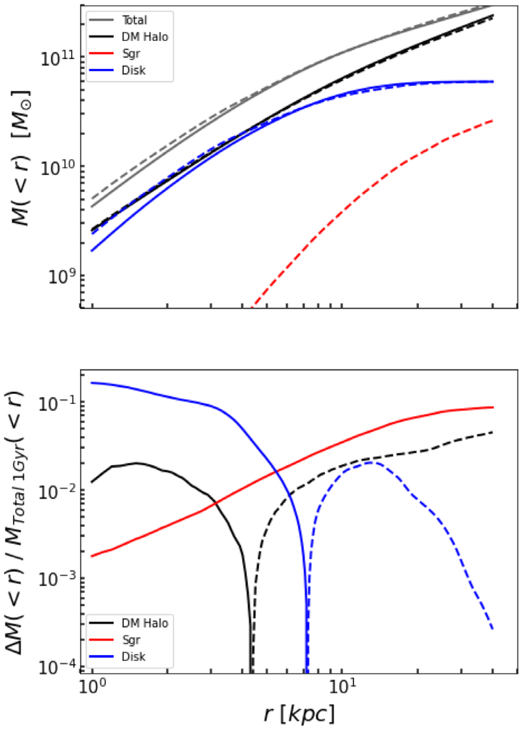

Figure 3. Mass evolution as an indicator of the scale of overall net acceleration contributions ($\sim GM(<r)/r^2$) and changes to those contributions. *Top*: Total mass $M(<r)$ enclosed within spherical radius r (grey), as well as separate contributions from the DM halo, Sgr, and disc. For the separate components, the solid line indicates $M(<r)$ at $t = 1$ Gyr and the dotted line is for the end of the simulation. *Bottom*: Change between dotted and solid lines from top panel divided by the total $M(<r)$ at $t = 1$ Gyr (bold grey line from top panel). Solid lines indicate positive $\Delta M(<r)$ while dashed lines indicates negative $\Delta M(<r)$. Note the small evolution in the radial profiles, and even smaller contribution of Sgr debris to that change.

the $m = 0$, 1, and 2 Fourier terms in the left/middle/right columns, respectively. The rows show: (top) the absolute change in Σ, with the same colour bar as Fig. 4 for comparison; (middle) the per cent change relative to the unperturbed $m = 0$ term; and (bottom) the phase. Note that for the $m = 0$ term, the 'phase' simply indicates whether the change is positive (red) or negative (blue) since this component is, by definition, axisymmetric. In order to account for the numerical scatter, we smooth the amplitude values at each radius, R, using a simple moving median over a 0.12 Gyr window. The vertical line in all the panels indicate the times at which Sgr crosses the disc plane.

We use Epoch 0, before Sgr's first disc crossing at $\sim$ 2.5 Gyrs, to characterize the natural, self-gravitating response of the disc component to infinitesimal perturbations within the combined disc/halo system. In the real MW these could be due to (e.g.) Giant Molecular Clouds or dark matter subhalos. In the simulations we can see 'ringing' in the $m = 0$ term left over from the initial conditions, with enhancements (red in bottom left-hand plot) and deficits (blue) in Σ propagating outward, with oscillation periods that increase with radius. There is also a response in the $m = 1$ term, which is clear in amplitude in the outer disc and steadily oscillating phases at all radii. It is intriguing to note that the phases follow a blue-black-red-white sequence in the inner disc (indicating retrograde pattern rotation) but red-black-blue-white sequence in the outer disc (indicating prograde pattern rotation). The change from retrograde to prograde occurs around $R \sim 10 - 15$ kpc, where the rotation curve is flat, most dominated by the disc self-gravity and transitioning between the inner rigid body and the outer gently-falling behaviour as it becomes halo-dominated. The $m = 2$ term shows hints of oscillating phase within $\sim$5kpc, but the amplitude associated with that oscillation is too low for a conclusive identification to be made.

During subsequent Epochs, Fig. 5 shows some patterns that are common to all Fourier terms. The influence of Sgr's disc crossings is immediately apparent in all panels as an increase in amplitude and re-alignment in phase (vertical colour-bands coincident with the dotted lines). The only exception is the third disc crossing at $\sim$4.5 Gyrs which occurred at Sgr's orbital apocenter, well beyond the disc extent. After each crossing, the longer dynamical time-scales and slower natural oscillations of the outer disc can be seen in both amplitude and phase as diagonal ridges tipping further and further away from vertical alignment until they are reset by the next interaction. Within $R \sim$5 kpc, where the rotation curve is closer to rigid body and the axisymmetric bulge has some influence, the oscillation amplitudes are smaller and there is a tendency to maintain alignment in phase.

On the other hand, some features of evolution are unique to each term.

For the $m = 0$ term, the time-scale for oscillation is shorter than for the higher order terms (notice that the blue ridges are more closely spaced in time in the bottom left-hand panel compared to the bottom middle and right-hand panels), as a reflection of the higher frequencies in the radial and vertical directions (governing axisymmetric ringing in density) compared to the differences in frequencies in the azimuthal direction (governing winding of non-axisymmetric patterns – summarized in bottom panel of Fig. 1). The $m = 0$ term also shows the net migration of material around the disc (see Fig. 3) as it is dominated by a decrease/increase in the disc surface density in the inner/outer disc (blue/red in phase) after $\sim$5.5 Gyrs.

The $m = 1$ term reveals the same retrograde intrinsic mode in the inner disc seen during Epoch 0. It is replaced by a global prograde pattern for a short period following the second disc crossing at $\sim$2.5 Gyrs, but subsequently resumes. The prograde pattern incited by the disc crossing remains dominant in the outer disc during Epoch 1, but has a lower oscillation frequency than that seen during Epoch 0, and is therefore likely of a different nature. The red curves in Fig. 6, which follow:

$$\phi(R, t) = \phi_{\rm cross} + \frac{v_{\rm circ}(R)}{R}(t - t_{\rm cross}), \tag{3}$$

where $t_{\rm cross}$ and $\phi_{\rm cross}$ are the time and phase angle (the same for all radii) at disc crossing, suggest that the phase evolution is consistent with a local disturbance simply winding up due to the differences of azimuthal time periods with radius, so it can be attributed to phase mixing.

The $m = 2$ term, in contrast to the dual nature of the $m = 1$ response, shows changes that are initially aligned in phase at all radii, winding up in smoothly and continuously at all radii to form spiral arms. The red curves in the bottom panel of Fig. 6 (which are repeated from the top panel) show that the winding up of this pattern is slightly slower than that expected from phase-mixing alone, demonstrating the importance of self-gravity in sustaining the spiral arms. The power in this term increases dramatically at the center of the disc towards the end of the simulation, with the aligned phases reflecting the presence of a steadily rotating bar (e.g. around 6 Gyrs).

The behaviour in the $m = 2$ term seen in our simulations is reminiscent of earlier work by Purcell et al. (2011), which pointed out how Sgr might instigate the formation of the MW's spiral pattern. As

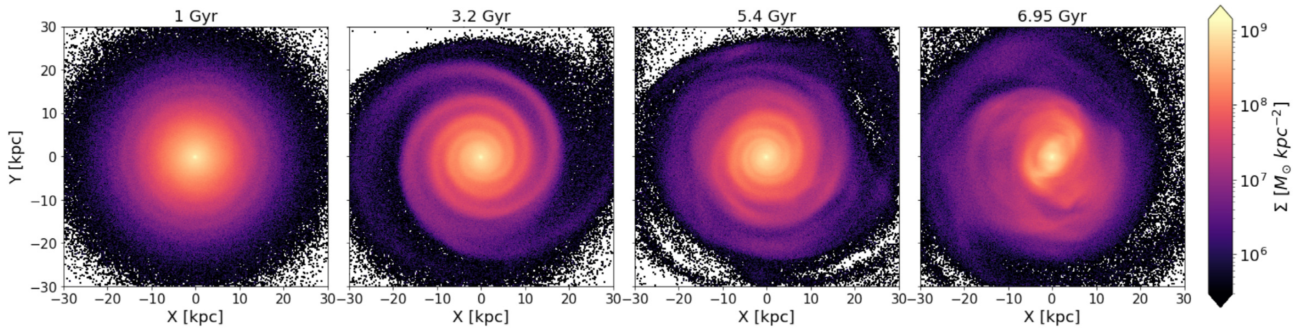

Figure 4. Panels each show an example of the disc's surface density from each Epoch in the simulation. They have has separate morphological characteristics, going from isolation to spiral arm formation, to a phase of winding spiral arms, and finally mostly complex structure with the bar forming in the inner disc.

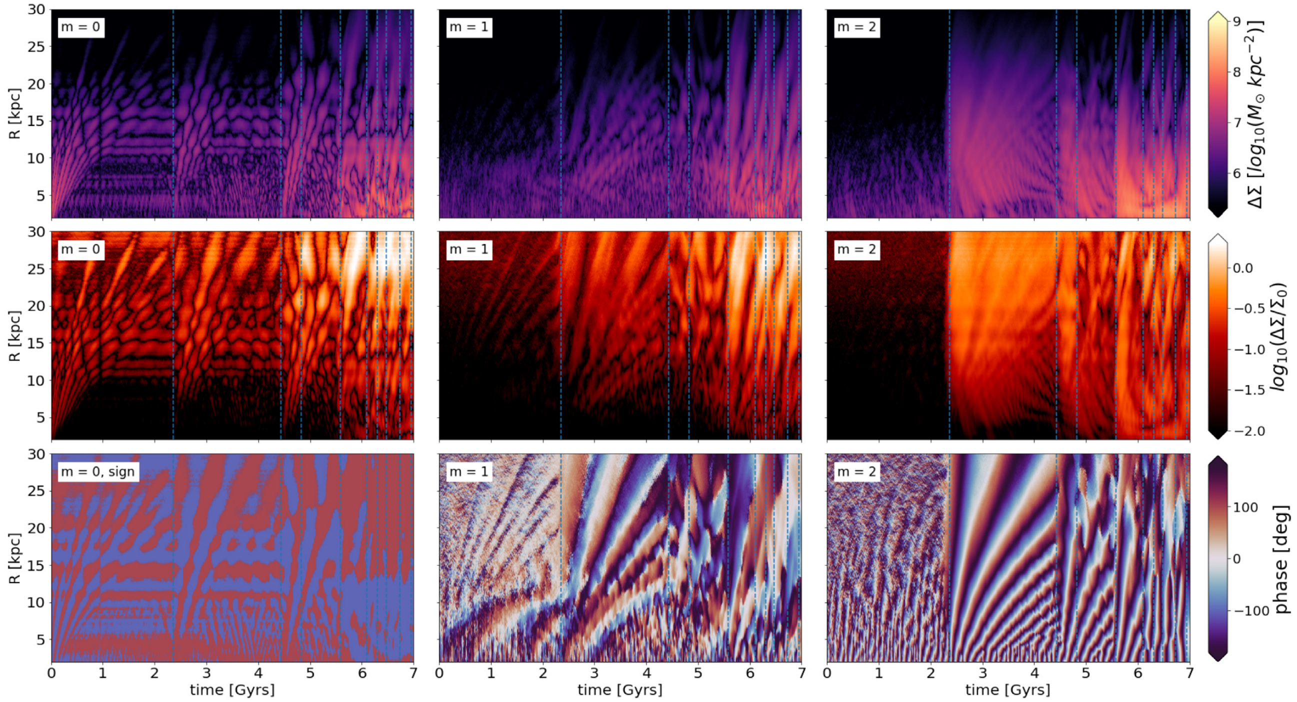

Figure 5. Amplitudes and phases respectively of the spatial Fourier terms for the m = 0 (first column), m = 1 (second column), and m = 2 (third column) terms in changes to the disc surface density ($\Delta\Sigma$). The amplitude for the m = 0 term is coloured as the difference in amplitude from the snapshot at 1 Gyr, which we define as the isolation snapshot ($\Delta\Sigma = \Sigma - \Sigma_0$). Rows are then organized as density (top), percentage change from the isolation snapshot ($\Delta\Sigma/\Sigma_0$, middle), and phases (bottom panel). Vertical dashed lines represent impact events with Sgr, and the 'phase' in the bottom left-hand panel indicates the sign of the $m = 0$ amplitude.

shown by Kyziropoulos et al. (2016), this conclusion about the arms being externally excited rather than plausibly arising from purely internal, secular effects, depends on the combined properties of Sgr and the parent. In our simulations, each disc passage plainly seeds a new set of Σ perturbations, so the satellite is clearly responsible.

4 RESULTS II: ANALYSIS OF INFLUENCES

We now turn to looking at the net influences on the disc in the context of our understanding of the evolution of Sgr's orbit and mass (Section 3.1), the (low-level) of global redistribution of matter in all components (Fig. 3) and the characteristics of the disc response (Section 3.2). We first examine the discs own self-gravity (Section 4.1), before comparing the accelerations due to all the Galactic components (Section 4.2). We summarize the results in the different temporal Epochs and spatial Regimes in Section 4.3.

4.1 Disc self-gravity

Fig. 7 shows nine pairs of panels to summarize the amplitude (upper panel of each pair) and phase (or sign for the $m = 0$, lower panel of each pair) of the Fourier decomposition of the acceleration in the galactic plane due to disc particles. The columns show the different dimensions, Δa_R, a_ϕ, a_z, and the rows separate out the terms, $m =$ 0, 1, and 2.

4.1.1 Accelerations within the disc plane

The in-plane accelerations, Δa_R and a_ϕ, can be directly related to the evolution of surface density apparent in Fig. 5 and discussed in

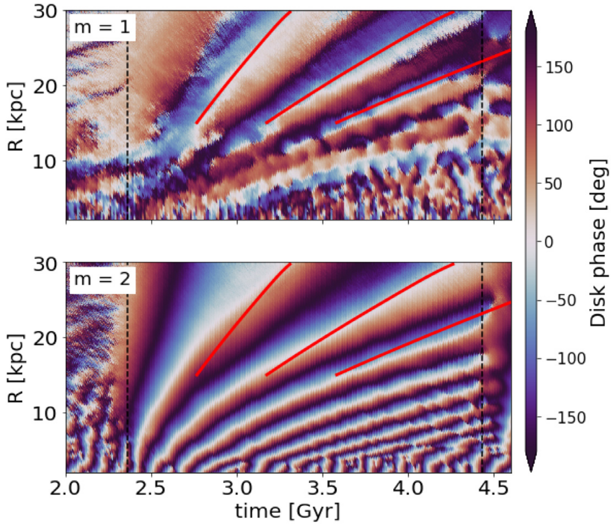

Figure 6. *Top:* Zoom-in of the m = 1 phase of the disc during Epoch 1 (2.3–4.4 Gyrs). Over-plotted as a red line starting at $R = 15$ kpc is the prediction for the phase given by the rotation curve presented in Fig. 1. Black vertical lines represent Sgr passages. *Bottom:* Same as top panel but for the m = 2 phase.

Section 3.2. All panels show clear association of sudden changes to the acceleration fields at disc passages.

The $m = 0$ terms amplitude and sign reflects the outward propagating rings in density during the early part of the simulation. Towards the end, it is dominated by the net change in mass distribution, which results in a decrease/increase (red/blue) in the attractive force in the inner/outer disc.

The $m = 1$ term follows the slow, retrograde pattern seen in density in the inner disc for much of the simulation. Since much of the mass is in the inner disc, the accelerations are also dominated by this sense of rotation in the outer disc, in contrast to the prograde pattern seen in density. There is an enhancement in the $m = 1$ amplitude in the inner disc (< 5 kpc) between the 5th and 6th passages, right before the bar is formed.

The $m = 2$ term has a prograde pattern at all radii, with new generations of spiral arms excited at each passage and subsequently winding up. The accelerations in this term are most strongly excited by the passages in regions that are localized in radii and that drift inward with each passage. The amplitude following each passage damps more quickly (in less than a Gyr) than the lower order terms. The inner few kpc are more clearly dominated by aligned accelerations throughout the simulation, with power increasing, and pattern speed falling in the last 1.5 Gyrs as the bar forms.

4.1.2 Accelerations perpendicular to the disc plane

We can directly relate the right-hand panels for the acceleration perpendicular to the plane a_z, to the decomposition of the vertical structure of the disc of the same simulation by Poggio et al. (2020a) and Laporte et al. (2018a). They discussed the structures they found in terms of bending waves, a warp, and the formation of a bar. The amplitudes in all three terms are strongly excited for a short period following each disc passage in a localized region that drifts inward in radius over time – reminiscent of the $m = 2$, in-plane accelerations.

The $m = 0$ term shows the bending modes in the outer disc that have been studied in great depth elsewhere (Widrow et al. 2014), clearly excited by each Sgr disc crossing.

In the $m = 1$ term, there are signatures of the evolving and outwardly moving warp between 2 and 4 Gyrs, which is slowly precessing in a retrograde direction (see Poggio et al. 2020a, for a detailed discussion). Note that, unlike the surface density, the vertical oscillations further in remain aligned in phase, indicating the same frequency for a broad range of radii. Between the 4th and 5th disc crossings, there is also power localized in the inner parts (∼5 kpc) of the disc, suggestive of an instability which we will return to in the following sections.

In the $m = 2$ term, we see the repeated pattern of the passage of Sgr inducing vertical waves, initially aligned in phase that subsequently decay, and wind up over time. The $m = 2$ motion is distinct from the $m = 1$ warp as the phase-plots indicate that the pattern is prograde rather than retrograde and rotates at a much higher speed. A comparison of the phase-plot (bottom right) with the equivalent panel for a_R (top left) suggests that the time-scale for winding the pattern in Z is slightly longer (white lines spaced further apart). This is likely because the in-plane natural phase-mixing frequency ($=\Omega - \kappa/2$) is higher than that for vertical oscillations ($=\Omega - \nu/2$, see Poggio et al. 2020a, for an in-depth discussion).

4.2 Comparison of disc, satellite, and halo accelerations

Plots equivalent to Fig. 7 which include the phases of the Fourier decompositions of accelerations due to Sgr and the DM halo are presented in Appendix A. In this section, we focus on comparing the amplitudes alone, within (Section 4.2.1) and perpendicular to the Galactic plane (Section 4.2.2).

Fig. 8 illustrates our visualization technique for the example of one dimension of acceleration (a_z) and one Fourier term ($m = 0$). Each of the upper panels shows the amplitude of this Fourier term at each radius (y-axis) and over time (x-axis), covering the entire simulation. Sgr, the DM halo and the disc are shown using blue, green, and red colour intensity to represent that amplitude of their influence, respectively. In the lower panel, the colours are combined in proportion to the amplitudes from the separate components, with the saturation indicating the combined amplitude (see colour wheel on the bottom right of the figure). We will refer to this as the RGB panel (Red-Blue-Green panel) for all subsequent plots. In the RGB panel, red regions indicate where the disc dominates much more than the other components, while yellow regions indicate where the disc and DM halo influences are comparable to each other. Areas in which all three components have a high amplitude – i.e. high saturation in their respective colours – are close to white. On the other hand, areas where the combined influence is low will lead to darker, less saturated colours that are closer to black (e.g.the outer disc during the first Gyr). While there is an immense amount of information in these plots, our use of them will be confined to broadly assessing the importance of the different components in different Epochs (i.e. time) and Regimes (i.e. space). A summary of the RGB panels of the following figures, which allows the reader to compare them all directly, can be found in the Appendix (A3).

4.2.1 Accelerations within the disc plane

Figs 9 and 10 show the Fourier decomposition of the radial and azimuthal influences within the disc plane, with each column corresponding to the $m = 0/1/2$ terms. Rows 1/2/3 represent the tidal influences of Sgr, the DM halo, and the disc's self-gravity (repeated from Fig. 7), respectively, and the bottom row shows the RGB panels.

The broad characteristics of the top two rows in both figures clearly reflect our physical intuition for the intertwined evolution of Sgr and

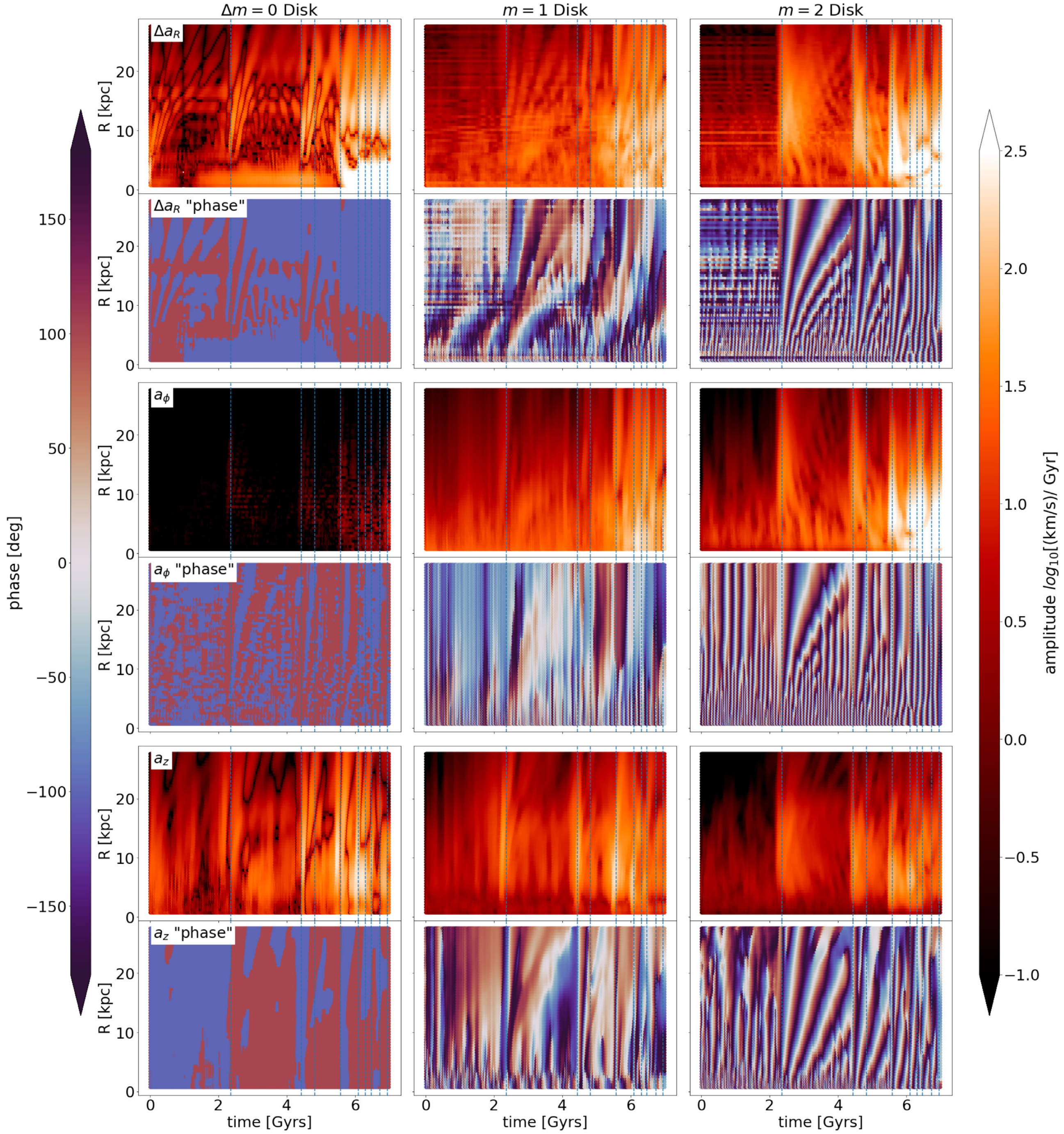

Figure 7. Amplitudes and phases for accelerations due to disc self-gravity. Columns are $\Delta m = 0$, $m = 1$, and $m = 2$, respectively. Rows are the amplitude/phase pairs for Δa_R, a_ϕ, and a_z accelerations, respectively. We note again that the $m = 0$ 'phase' is simply an indication of its sign.

the dark matter halo. Sgr's influence has sharp peaks around each of the plane crossings. The small size of Sgr relative to the disc means that its influence is limited in radius and azimuth, and all three Fourier terms are needed to capture this localization. The speed of its passage limits its peak influence to $\sim\pm 100$ Myrs around each plane crossing. The third plane crossing just before $t = 5$ Gyrs is unimportant as it occurs near Sgr's apocenter far beyond the edge of the disc.

The dark matter halo responds more ponderously, with the overall contraction and expansion as Sgr dives in and out of its central regions captured in the $m = 0$ term of the in-plane radial acceleration. (The sign changes accompanying this can be seen in the $m = 0$ panels in Fig. 9). The distortion of the dark matter halo due to Sgr is predominantly captured in the $m = 1$ term, with little contribution from $m = 2$. This distortion lags the disc crossing seen in the Sgr panels, and effectively extends the external non-axisymmetric perturbations to the disc from 100 Myr to ~Gyr time-scales. Both these external perturbations move deeper into the disc over time as Sgr's orbit decays due to the energy and angular momentum exchange between the components.

In contrast to Sgr and the DM halo, the disc's distribution of near-circular orbits supports coherent, rapidly rotating and mixing responses seen in density, and their corresponding accelerations.

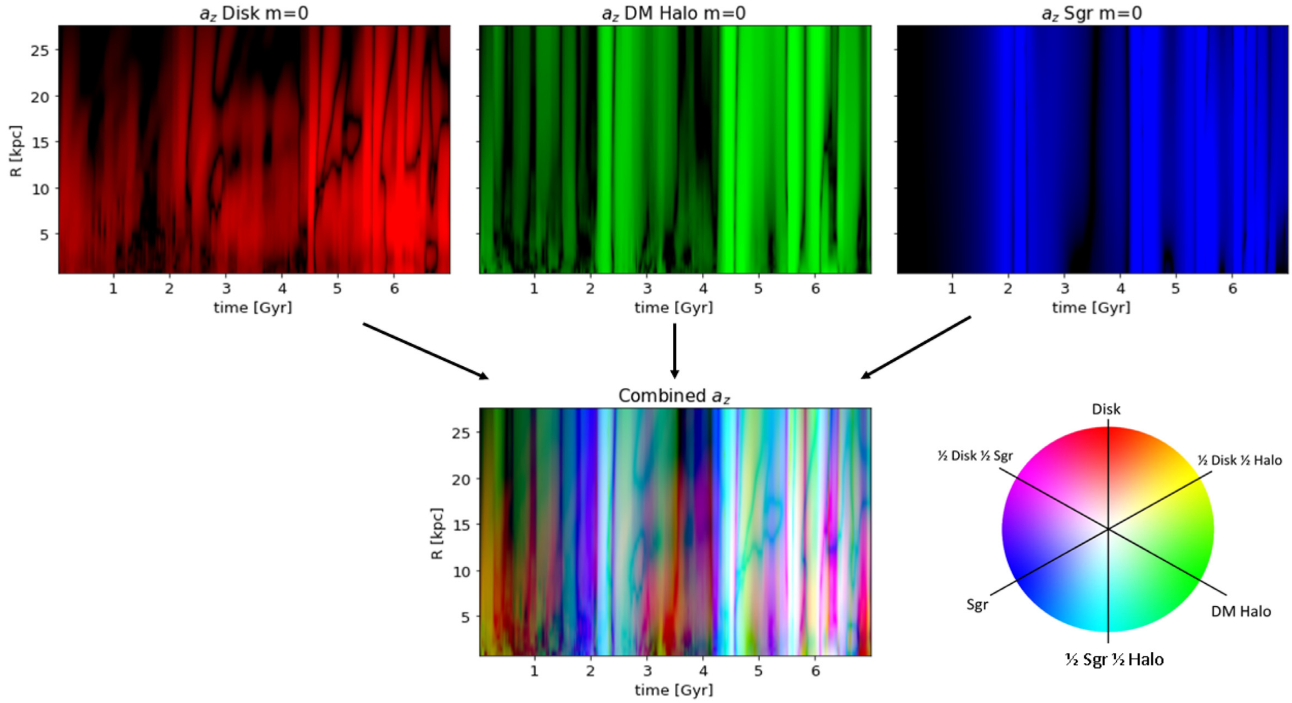

Figure 8. Illustration of how the bottom 'RGB' panels in Figs 9–11 are constructed using the a_z m = 0 as an example. Disc self gravity is coloured as red, while the tidal accelerations from the DM Halo and Sgr are coloured green and blue, respectively. In the bottom panel is the resulting combined panel by simply adding these together. Areas with high saturation from multiple components – such as the combined influence from Sgr and the DM Halo at time = 2.5 Gyr – result in a white hue, while low saturation are black. Red/blue/green colours indicated times and regions where the disc/Sgr/DM halo dominate the acceleration, respectively.

These are clearly instigated by each passage and decay over tens of orbital periods, as noted in the prior section.

The bottom RGB panel summarizes the relative importance of each of these contributors. The blue hue from Sgr is clearly visible at every disc passage in every panel of both figures. The importance of the distortion of DM halo in enhancing the torque on the disc is apparent as extended green colours in the $m = 1$ panels following each Sgr disc crossing (as recognized in many prior works Weinberg 1998; Weinberg & Blitz 2006; Gómez et al. 2013; Laporte et al. 2018a). The increasing relevance of $m = 2$ patterns in the disc – presumably the spiral arms and the bar seen in Fig. 4 – can be seen in red, in particular in the bottom right panel.

4.2.2 Accelerations perpendicular to the disc plane

Fig. 11 repeats Figs 9 and 10 for the a_z component of accelerations due to each galactic component.

As with the earlier figures, Sgr's influence (top row) is confined to a narrow window around each of the disc crossings and is apparent in each Fourier term. The characteristics of the left column can be simply related to Sgr's motion, as it orbits perpendicular to the disc in a plane almost aligned with the x-axis. The abrupt zeros in amplitude (black) in every panel reflect this geometry as Sgr plunges in sequence down and up through the $z = 0$ plane. (This can also be seen explicitly in the associated phase-plots in Fig. A1.) Over time, the influence becomes ever more localized in radius as Sgr's orbit decays and the crossings occur within the disc itself.

In contrast to Sgr, the DM halo's influence perpendicular to the plane (second row of paired panels) is largely captured by the $m = 0$ term alone as it responds to the much smaller intruder, and pulls vertically on the galactic disc. This response noticeable lags the crossing time. Nor is it strictly confined to the disc passages, but rather takes ~1 Gyr to settle following each encounter. The much lower power in the higher order terms suggests that the DM halo does not tilt significantly relative to the disc despite Sgr's influence.

Nevertheless, the combination of Sgr and the DM Halo does instigate bending in the disc. This is captured by localized power in both the $m = 1$ and $m = 2$ terms (third row of panels), coincident with Sgr's passages. The self-gravity of this bending is far more important than the DM halo's external influence in these terms. It extends the influence of vertical forces beyond Sgr's disc passages, and exceeds the amplitude of those impulsive perturbations by the end of the simulation.

The RGB-panel demonstrates that in the z direction, the DM halo's response to Sgr (green) is most apparent in the $m = 0$ term, effectively extending the duration of net vertical accelerations beyond each crossing. The self-gravitating influence of bending of the disc (red) is important in the $m = 1$ and $m = 2$ terms only for a short time following earlier passages, but becomes increasingly relevant as Sgr's orbit decays. In particular, note the red hues around $R \sim 5$ kpc in $m = 1$, which suggest significant instability in the inner disc. Sgr's influence around the disc crossings for these higher order terms is indicated by the violet hues at those times.

4.3 Comparison of influences in temporal epochs and spatial regimes.

Figs 9–11 provide a visual overview of how each component influences the disc, in what region, over what time-scale and in which Fourier term. As a quantitative comparison of the significance of these different influences on disc, Figs 12–14 show the amplitude of Fourier terms in the outer (25 kpc), middle (10 kpc), and inner

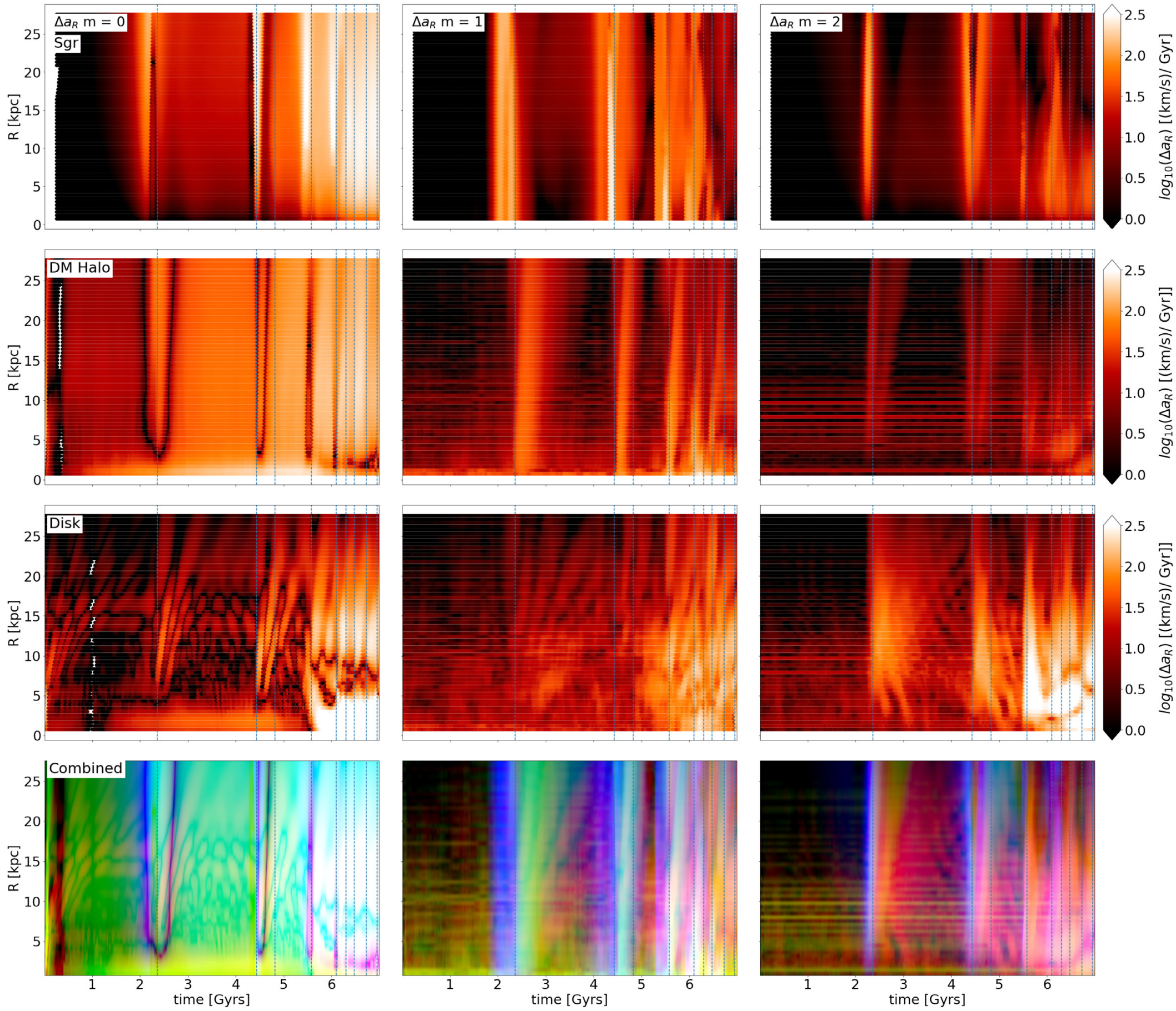

Figure 9. Fourier decomposition for the radial acceleration from each component on the disc plane. The x- and y-axis for each subplot are time (Gyrs) and cylindrical radius away from galactic center (kpc), respectively. The columns shows the amplitude of the m = 0/1/2 terms with the vertical dashed lines indicating Sgr disc crossings. Rows in the figure show accelerations in the disc plane due to Sgr (top), the DM Halo (second), and the disc (third). The bottom row shows the combined influences of all three (as in Fig. 8).

(2 kpc) disc, respectively. The columns show the three cylindrical acceleration components (a_z, a_ϕ, and a_R) and the rows are the first three Fourier terms ($m = 0$, $m = 1$, and $m = 2$). The values are presented as fractions of the radial $m = 0$ acceleration of the corresponding ring at time = 1 Gyr. Each component's amplitude is plotted together in order to compare their relative strength as a function of time and radius (Sgr in red, the DM halo in black and the disc in blue). As before, for the $m = 0$ terms in these figures, we plot the change in amplitude with respect to the conditions at time = 1 Gyr.

Fig. 12, showing accelerations in the outer Galaxy, emphasizes how this region of the disc is sculpted by the twin influences of Sgr and the DM halo. The mass in disc stars is sufficiently low that its self-gravity is largely negligible in this region until its center becomes non-axisymmetric towards the end of the simulation. In the z-direction, Sgr is dominant in all Fourier terms. As our expansion is centered on the plane defined by the disc stars, we can see how the offset of the disc from the DM halo's symmetry plane is apparent as an acceleration in the z-direction in the apposite direction to Sgr, lagging behind the passages. The non-axisymmetric distortion of the DM halo (the 'wake') induced by Sgr contributes significant amplitude in the $m > 0$ terms for both a_ϕ and a_R that extends beyond the influence of Sgr alone at the disc crossings, as anticipated and demonstrated from prior work (Weinberg 1998; Weinberg & Blitz 2006; Gómez et al. 2016; Laporte et al. 2018b). The steady decrease in the $m = 0$ DM halo contribution stems from the center of the halo being heated by the combined interactions and becoming more diffuse.

Fig. 13 repeats Fig. 12 but for a ring 10 kpc away from the galactic center. In this region, Sgr, the disc, and the DM halo all exert significant influences. In the z-direction, the amplitude of the disc oscillations reveal the presence of bending modes (in $m = 0$), a warp (in $m = 1$, coincident with the DM halo response), and a phase-mixing $m = 2$ vertical oscillation. In the azimuthal direction, the extended DM halo torque is again apparent in $m = 1$, while the formation of spiral arms can be seen in $m = 2$. In the radial direction,

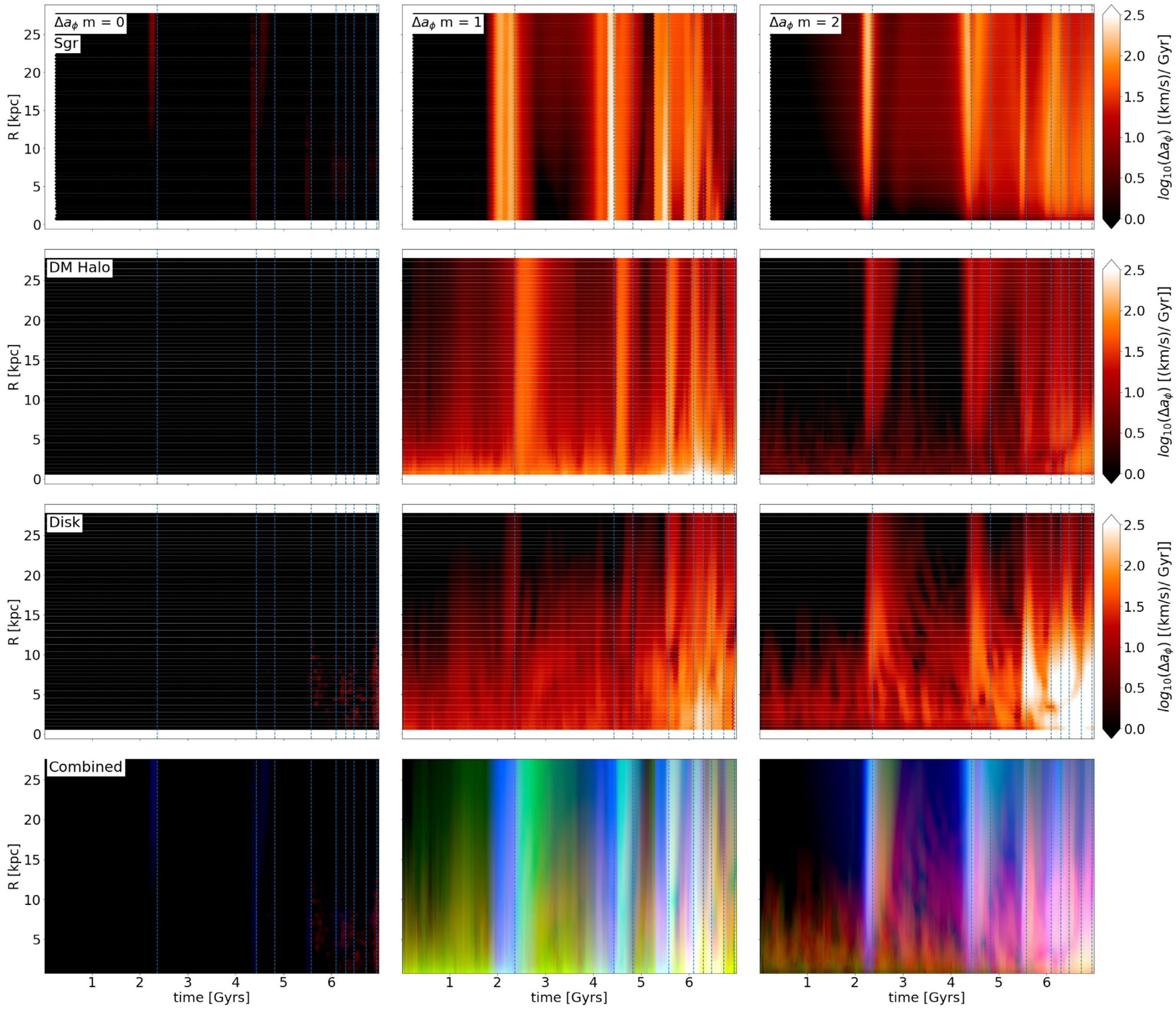

Figure 10. Fourier decomposition of the azimuthal acceleration from each simulation component on the disc plane. Setup the same as Fig. 9. The m = 0 column has an amplitude approximately equal to zero because the m = 0 mode is, by definition, axisymmetric and so will have no signal in the azimuthal acceleration.

the (mild) expansion of the middle parts of both the DM halo and disc are apparent in $m = 0$ (see Fig. 3), as well as the decrease in the Galactocentric radius of Sgr. The $m = 1$ and $m = 2$ terms for the disc suggest the increasing importance of a bar as it is increasingly destabilized by repeated Sgr passages.

Fig. 14 repeats Figs 12 and 13 for a ring in the inner disc, at 2 kpc from the galactic center. In this region, while the evolution is driven by the Sgr impacts, disc self-gravity dominates the acceleration fields. In particular, the spike in the amplitude of the a_z, $m = 1$ term in the disc following Sgr's disc passage at $t \sim 5.6$ Gyr suggests that this is the disc instability event that led to the formation of the Galactic bar whose presence is clear following this passage in the $m = 1$ and $m = 2$ terms in a_ϕ and a_R (see Petersen, Weinberg & Katz 2019; Weinberg & Petersen 2020, for an in depth description of this process).

5 SUMMARY AND CONCLUSION

Many prior studies have shown that it is impossible to understand the response of a galactic disc to the gravitational influence of a satellite galaxy without taking a holistic view – one that accounts for the mutual interactions of all galactic components (Weinberg 1998, 1999; Vesperini & Weinberg 2001; Weinberg & Blitz 2006; Gómez et al. 2016; Laporte et al. 2018a,b; Garavito-Camargo et al. 2020). The passage of the satellite distorts the DM Halo surrounding the disc; this distortion enhances the influence on the disc both directly and by causing the orbit of the satellite to decay; and the disc's own self-gravity can drive its further evolution. Even the MW – a relative quiet backwater in the Universe – shows abundant signatures of these ongoing actions and reactions (Widrow et al. 2012; Williams et al. 2013; Amôres et al. 2017; Antoja et al. 2018; Binney & Schönrich 2018; Bland-Hawthorn et al. 2019; Chen et al. 2019; Laporte et al. 2019; Skowron et al. 2019; Laporte, Koposov & Belokurov 2021), which could potentially tell us much about how the components are interacting. However, disentangling the interlocked causes of these signatures remains a challenge to the field.

In this work, we have presented a new approach to studying this complexity. We mapped accelerations caused by the three main protagonists (Sgr, Galactic disc, and DM halo) on to the Galactic disc in the radial, azimuthal, and vertical directions. The mapping allows us to determine the impact of each player (and therefore which one is

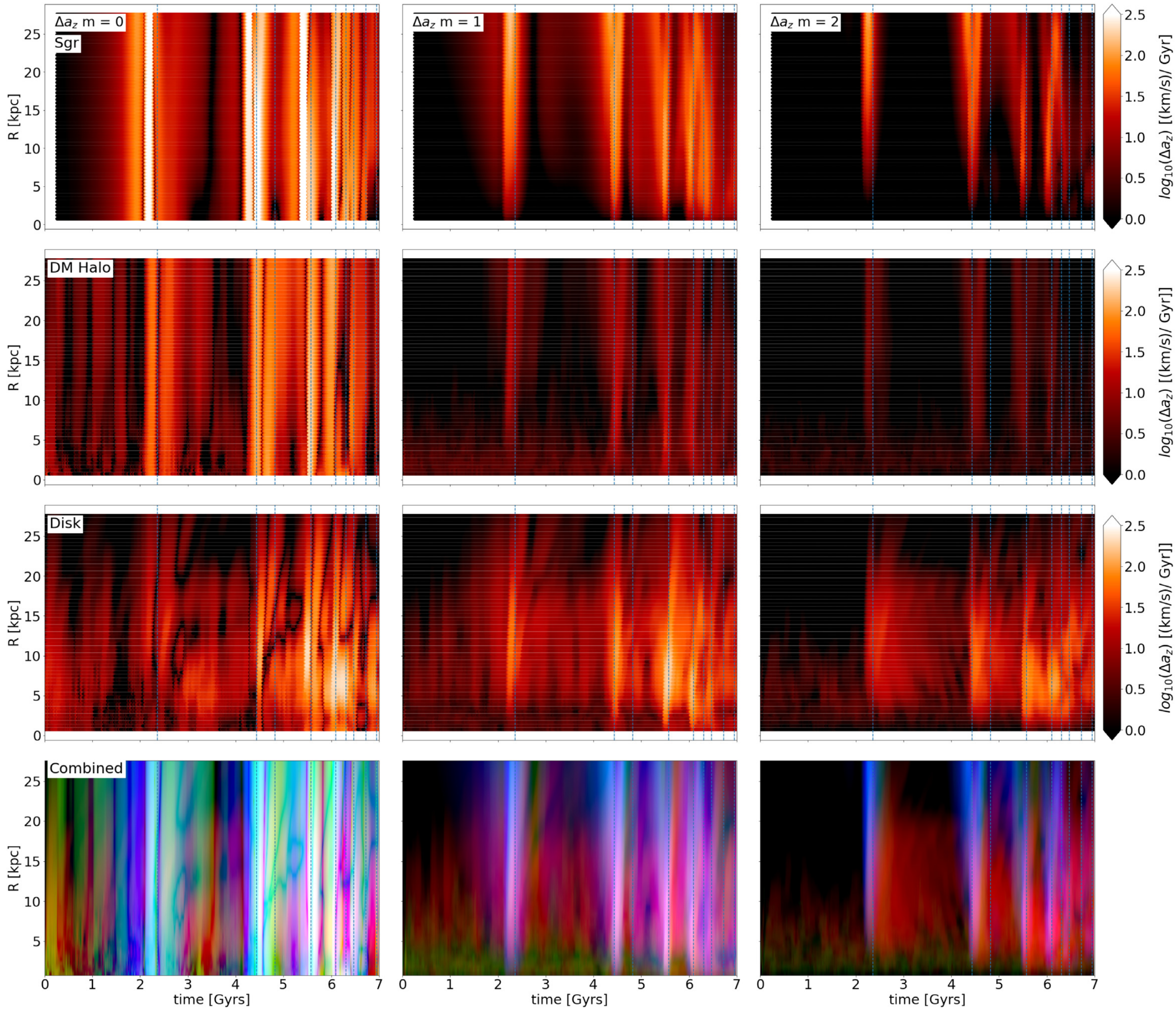

Figure 11. Fourier decomposition of the vertical acceleration from each simulation component on the disc plane. Setup the same as Fig. 9.

dominant) at a given position in the Galactic disc and at a given time throughout the simulation, providing a unique view on the causal connections driving the evolution of the Sgr-MW system. We have shown how each different component's influence on the disc can lead to the asymmetries present in our galaxy and how some signatures are more heavily dominated by one component over another.

Fig. 15 presents a schematic to summarize our results. It tabulates the nature of the dominant influences (source, Fourier term, and dimension), response (in italics) and interaction regime (square brackets) for different disc regions (rows) and within each temporal epoch identified in Section 4. For instance, during 3rd epoch (4.4–6.1 Gyrs), we have three different interaction regimes depending on which spatial region of the disc we analyse.

The figure emphasizes that each component – Sgr, the DM halo, and the disc – shapes the disc in distinct and characteristic ways in space and time.

(i) **Sagittarius** directly dominates accelerations only for $\pm 100-300$ M years (depending on radius) around plane crossings at small enough radii to impact the disc, exciting longer-lived, slowly decaying modes in the disc. Its direct influence is particularly important during the first few encounters while it still has a mass $\sim$2–$6\times10^{10}\,M_{\odot}$, and in the intermediate-outer disc where the encounter time-scale is longer.

(ii) **The Dark Matter Halo distortion** ('wake') enhances and extends the direct influence of the much smaller dwarf, both in $m=0$ vertical acceleration and as $m=1$ in plane accelerations. These distortions are the dominant influence on the outer disc, driving the formation and evolution of the warp.

(iii) **The self-gravity of the disc response** becomes increasingly important at smaller radii and as the interaction progresses. The scale of accelerations due to bending waves in the middle-disc rivals the importance of the initial disturbance itself. The inner disc clearly becomes unstable in $m=1$ vertical oscillations that lead to the formation of a bar ($m=2$ terms, aligned in phase) by 6 Gyrs.

Given the similarity of the simulations to the properties of the observed MW and Sgr, it is likely that this description represents the broad characteristics of the recent dynamical history of our own Galaxy. Of course, the details are not expected to exactly match for a multitude of reasons. For example, the extent of the influence of Sgr will depend on the details of its mass loss history and we have not

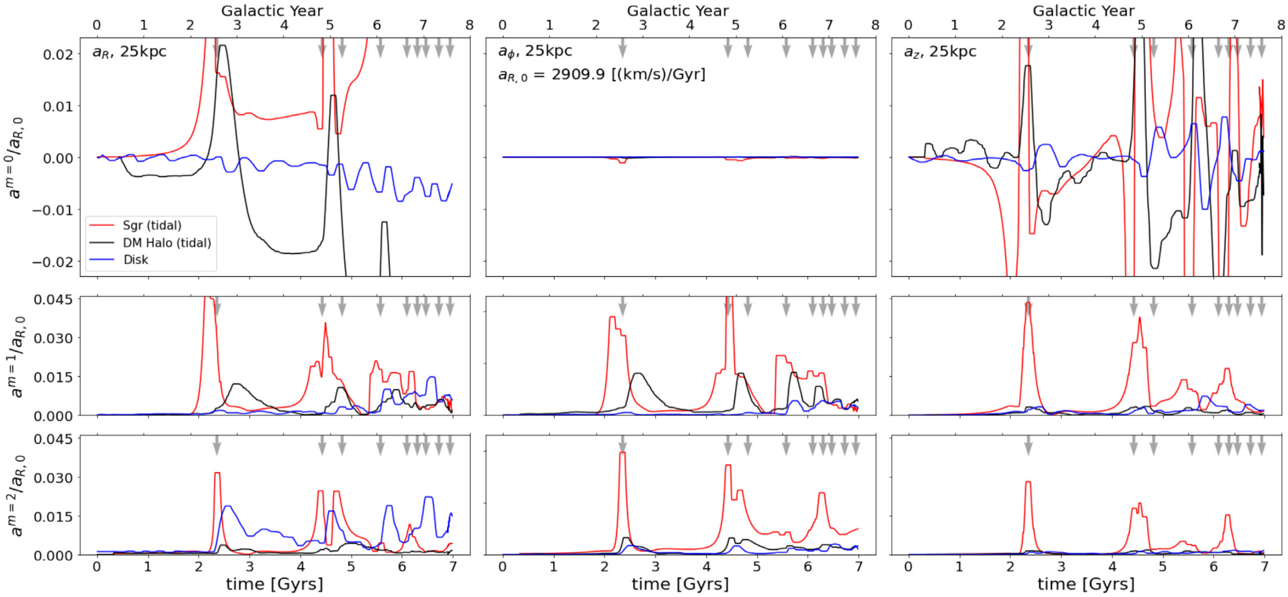

Figure 12. Fourier amplitudes for each cylindrical acceleration as a function of time. Amplitudes shown here are only for particles at a galactocentric radius of 25 kpc away from the center. The figure shows the first three Fourier modes for each acceleration term [a_R in the first column, a_ϕ in the second, and a_z in the last]. The modes are each normalized by the radial m = 0 value (summed from the DM halo and disc) of the corresponding ring at time = 1 Gyr. The normalization factor, $a_{R,0}$, is printed in the top middle panel. Each simulation component's Fourier amplitude is represented by a different colour: Sgr is coloured as red, the DM halo as black, and the disc as blue. Time is shown on the *x*-axis both in Gyrs (lower *x*-axis) and in galactic years (upper *x*-axis) for that particular radius – in this case 25 kpc. Arrows on the top of each panel show the time which a passage with Sgr occurs.

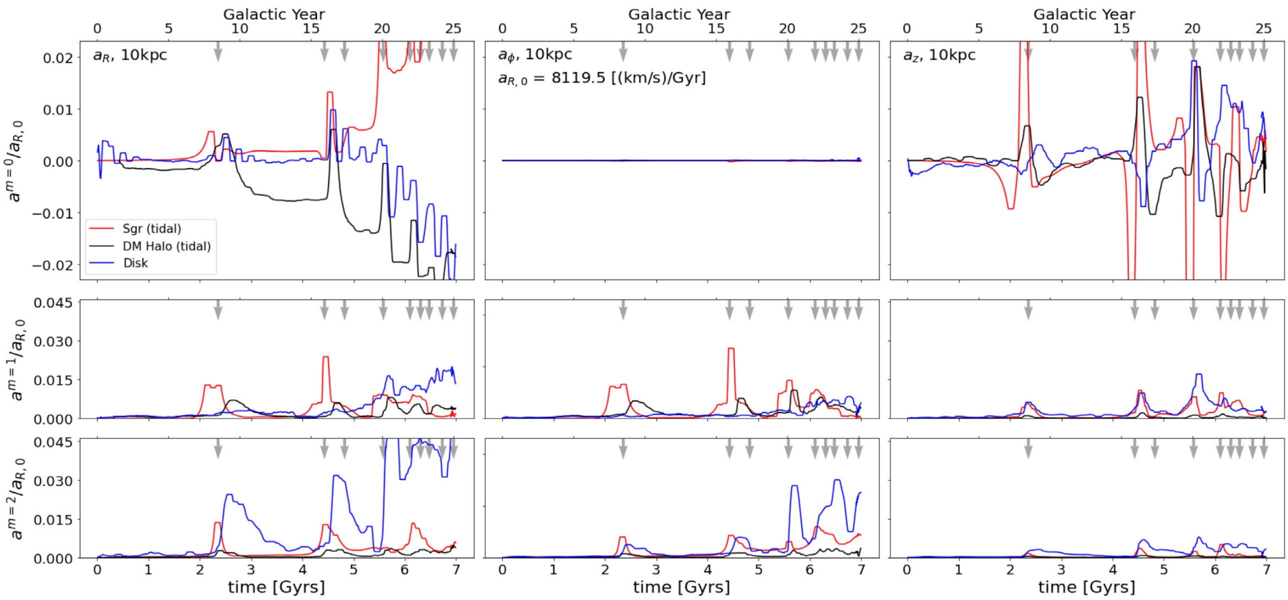

Figure 13. Fourier amplitudes at a constant radius as a function of time for particles 10 kpc away from the galactic center. Layout exactly the same as Fig. 12.

included the current influence of the LMC (expected to contribute equally to the outer disc, see Laporte et al. 2018a,b). In addition, our simulation assumed non-evolving disc and DM halo components, initially in equilibrium, while we might expect the MW to grow in scale and mass over several Gyrs and only just be recovering from its merger with Gaia-Sausage-Encedaelus (see Helmi et al. 2018; Koppelman et al. 2019; Lancaster et al. 2019; Myeong et al. 2019; Grand et al. 2020). This missing history in turn leads to a disparity between the suspected age of the MW's bar which is thought to be many Gyrs old (Bovy et al. 2019; Debattista et al. 2019) and the recent formation of the bar in the simulation, within the last Gyr.

Nevertheless, it is interesting to speculate on the implications of our work for our view of the MW today, as summarized by the orange column in Fig. 15, which corresponds to the 5th plane crossing in the simulation after ∼6 Gyrs of evolution. The inner disc is dominated by self-gravitating structures (e.g. the bar), likely built from its (second order) reaction to its own (first order) response to prior interactions. Prospects for dissecting the dynamics of the ongoing interaction are more promising at larger radii. In the middle region, with Sgr

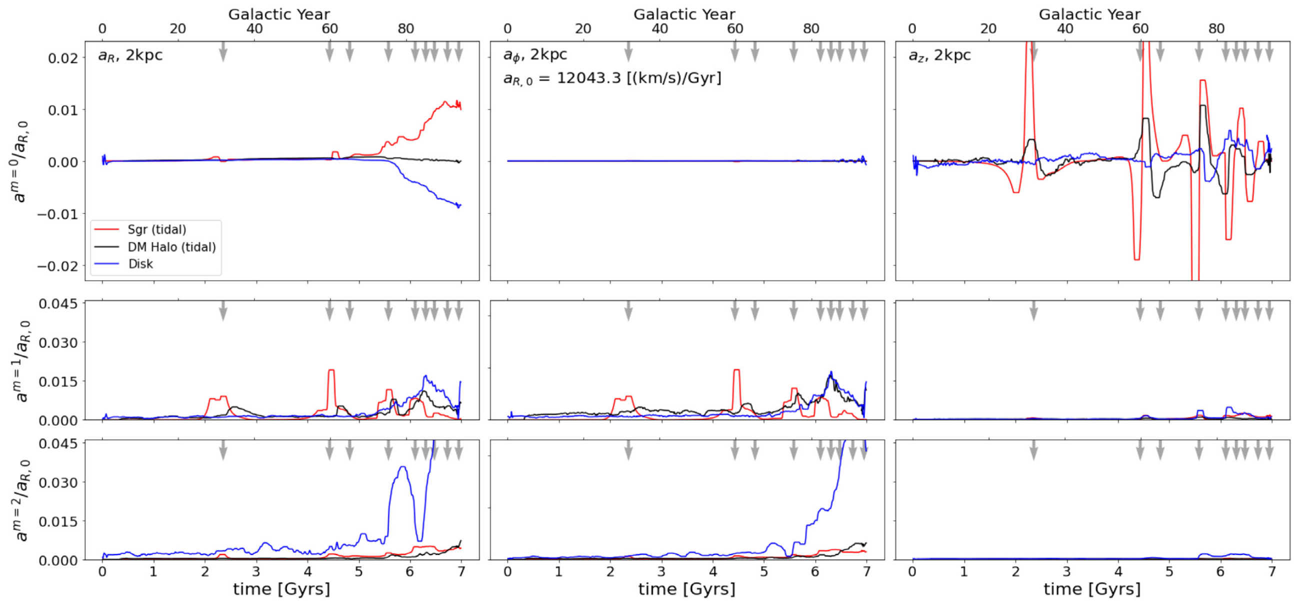

Figure 14. Fourier amplitudes at a constant radius as a function of time for particles 2 kpc away from the galactic center. Layout exactly the same as Figs 12 and 13.

Outer Disk (> 10kpc)	[Regime 0]	**DM halo** m=0: z, m=1: ϕ, R *wake, warp* **Sgr passages** [Regime 1]	**DM halo** m=0: z, m=1: ϕ, R *wake, warp* **Sgr passages** [Regime 3]	**Sgr, DM halo** m=0: z, m=1: ϕ, R [Regime 3]	**DM halo** m=0: z, m=1: ϕ, R *wake, warp* [Regime 3]
Middle Disk (5 – 10kpc)	[Regime 0]	**Disk** m=2: z, ϕ, R *spiral arms, bending* [Regime1]	**Disk** m=2: z, ϕ, R *spiral arms, bending* **Sgr passages** [Regime 1 and 2]	**Sgr, Disk** m=2: z, ϕ, R *spiral arms, bending* [Regime 3]	**Disk** m=2: z, ϕ, R *spiral arms, bending* [Regime 3]
Inner Disk (< 5kpc)	[Regime 0]	[Regime 0]	**Disk** m=1: z *bar formation* [Regime 1]	**Disk** m=2: ϕ, R *bar* [Regime 2]	**Disk** m=2: ϕ, R *bar* [Regime 2]
Epoch	**0 – 2.3 Gyrs**	**2.3 – 4.4 Gyrs**	**4.4 – 6.1 Gyrs**	**"Possible Present Day": ~ 6.1 Gyrs**	**6.1 – 7 Gyrs**

Figure 15. Summary of dominant perturbative influences. Bold font indicates source, regular font indicates Fourier term and dimension in each temporal epoch. Italics indicate physical consequences of the disturbances. Interaction Regimes defined in Section 3 are in square brackets: the disc evolving in isolation [0]; after a single impact [1]; during impacts repeated roughly every orbit [2]; during multiple impacts per orbit [3].

currently plunging through the disc of the MW (with an imminent plane-crossing in ∼25 Myrs – see Gandhi et al. 2021, for further discussion), we are entering a period which coincides with the peak of its influence and we most plausibly might catch the signature of the ongoing interaction directly. One approach could be to look at a global distortion to the disc's velocity field (see Laporte et al. 2019) before it has time to phase-mix away, although any interpretation will necessarily be complicated by the disc's own influence. Of course, the amplitude depends on the mass still associated with the dwarf. In our simulations, the mass of the dwarf at this point is sufficiently low that the disc's own self-gravity is more important, and recent estimates for the mass of the dwarf suggest it could be as low as (e.g. $5 \times 10^8\,M_\odot$; Vasiliev & Belokurov 2020). It is clear that the outer disc (e.g. Laporte et al. 2021) is the place to search for clues about the DM halo's distortion and previous impacts, though in reality the influence of both Sgr and the LMC will need to be taken into account in any interpretation (Laporte et al. 2018b).

We conclude that our holistic review of the interaction itself motivates the next step: a holistic review of the signatures of that interaction.

ACKNOWLEDGEMENTS

We would like to thank the Center for Computational Astrophysics in the Flatiron Institute for allowing us access to their binder server, making the management of the simulations much easier to share among the other members of this collaboration. We would also like to thank the members of both the Milky Way Stars group at Columbia and the Dynamics Group at the CCA, who consistently provided useful comments and suggestions for improvement of this work. In particular, we would like to thank Adrian Price-Whelan for greatly assisting in the creation of Fig. A3. We also acknowledge fruitful discussions with Martin Weinberg and Team Beefy. KVJ and DGF were supported by NSF grant AST-1715582. CL acknowledges funding from the European Research Council (ERC) under the European Union's Horizon 2020 research and innovation programme (grant agreement no. 852839). This work was supported in part by World Premier International Research Center Initiative (WPI Initiative), MEXT, Japan.

DATA AVAILABILITY

The data underlying this article were accessed from the binder cluster at the Computational Center for Astrophysics (CCA) at the Flatiron Institute. The simulated data used in this research will be shared on reasonable request to the corresponding authors.

REFERENCES

Amôres E. B., Robin A. C., Reylé C., 2017, A&A, 602, A67
Antoja T. et al., 2018, Nature, 561, 360
Bergemann M. et al., 2018, Nature, 555, 334
Binney J., Schönrich R., 2018, MNRAS, 481, 1501
Bland-Hawthorn J. et al., 2019, MNRAS, 486, 1167
Bland-Hawthorn J., Tepper-Garcia T., 2020, MNRAS, 504, 3168
Bovy J., Leung H. W., Hunt J. A. S., Mackereth J. T., García-Hernández D. A., Roman-Lopes A., 2019, MNRAS, 490, 4740
Burke B. F., 1957, AJ, 62, 90
Carlin J. L. et al., 2013, ApJ, 777, L5
Chen X., Wang S., Deng L., de Grijs R., Liu C., Tian H., 2019, Nat. Astron., 3, 320
Cheng X. et al., 2020, ApJ, 905, 49
Chequers M. H., Widrow L. M., 2017, MNRAS, 472, 2751
Chequers M. H., Widrow L. M., Darling K., 2018, MNRAS, 480, 4244
D'Onghia E., Madau P., Vera-Ciro C., Quillen A., Hernquist L., 2016, ApJ, 823, 4
Debattista V. P., Gonzalez O. A., Sanderson R. E., El-Badry K., Garrison-Kimmel S., Wetzel A., Faucher-Giguère C.-A., Hopkins P. F., 2019, MNRAS, 485, 5073
Djorgovski S., Sosin C., 1989, ApJ, 341, L13
Dubinski J., Kuijken K., 1995, ApJ, 442, 492
Eilers A.-C., Hogg D. W., Rix H.-W., Frankel N., Hunt J. A. S., Fouvry J.-B., Buck T., 2020, ApJ, 900, 186
Fragkoudi F. et al., 2019, MNRAS, 488, 3324
Fragkoudi F. et al., 2020, MNRAS, 494, 5936
Friske J. K. S., Schönrich R., 2019, MNRAS, 490, 5414
Gaia Collaboration, 2018a, A&A, 616, A1
Gaia Collaboration, 2018b, A&A, 616, A11
Gandhi S. S., Johnston K. V., Hunt J. A. S., Price-Whelan A. M., Laporte C. F. P., Hogg D. W., 2021, preprint (arXiv:2107.03562)
Garavito-Camargo N., Besla G., Laporte C. F. P., Price-Whelan A. M., Cunningham E. C., Johnston K. V., Weinberg M. D., Gomez F. A., 2020, preprint (arXiv:2010.00816)
Gibbons S. L. J., Belokurov V., Evans N. W., 2017, MNRAS, 464, 794
Gómez F. A., Minchev I., O'Shea B. W., Beers T. C., Bullock J. S., Purcell C. W., 2012, Boletin de la Asociacion Argentina de Astronomia La Plata Argentina, 55, 447
Gómez F. A., Minchev I., O'Shea B. W., Beers T. C., Bullock J. S., Purcell C. W., 2013, MNRAS, 429, 159
Gómez F. A., White S. D. M., Marinacci F., Slater C. T., Grand R. J. J., Springel V., Pakmor R., 2016, MNRAS, 456, 2779
Gómez F. A., White S. D. M., Grand R. J. J., Marinacci F., Springel V., Pakmor R., 2017, MNRAS, 465, 3446
Grand R. J. J. et al., 2020, MNRAS, 497, 1603
Helmi A., Babusiaux C., Koppelman H. H., Massari D., Veljanoski J., Brown A. G. A., 2018, Nature, 563, 85
Hernquist L., 1990, ApJ, 356, 359
Hunt J. A. S., Bub M. W., Bovy J., Mackereth J. T., Trick W. H., Kawata D., 2019, MNRAS, 490, 1026
Hunt J. A. S., Stelea I. A., Johnston K. V., Gandhi S. S., Laporte C. F. P., Bedorf J., 2021, preprint (arXiv:2107.06294)
Johnston K. V., Spergel D. N., Hernquist L., 1995, ApJ, 451, 598
Kawata D., Baba J., Ciucă I., Cropper M., Grand R. J. J., Hunt J. A. S., Seabroke G., 2018, MNRAS, 479, L108
Kawata D., Baba J., Hunt J. A. S., Schönrich R., Ciucă I., Friske J., Seabroke G., Cropper M., 2020, preprint (arXiv:2012.05890)
Kerr F. J., 1957, AJ, 62, 93
Khanna S. et al., 2019, MNRAS, 489, 4962
Khoperskov S., Di Matteo P., Gerhard O., Katz D., Haywood M., Combes F., Berczik P., Gomez A., 2019, A&A, 622, L6
Khoperskov S., Gerhard O., Di Matteo P., Haywood M., Katz D., Khrapov S., Khoperskov A., Arnaboldi M., 2020, A&A, 634, L8
Koppelman H. H., Helmi A., Massari D., Price-Whelan A. M., Starkenburg T. K., 2019, A&A, 631, L9
Kyziropoulos P. E., Efthymiopoulos C., Gravvanis G. A., Patsis P. A., 2016, MNRAS, 463, 2210
Lancaster L., Koposov S. E., Belokurov V., Evans N. W., Deason A. J., 2019, MNRAS, 486, 378
Laporte C. F. P., Gómez F. A., Besla G., Johnston K. V., Garavito-Camargo N., 2018a, MNRAS, 473, 1218
Laporte C. F. P., Johnston K. V., Gómez F. A., Garavito-Camargo N., Besla G., 2018b, MNRAS, 481, 286
Laporte C. F. P., Minchev I., Johnston K. V., Gómez F. A., 2019, MNRAS, 485, 3134
Laporte C. F. P., Famaey B., Monari G., Hill V., Wegg C., Gerhard O., 2020, A&A, 643, L3
Laporte C. F. P., Koposov S. E., Belokurov V., 2021, preprint (arXiv:2103.12737)
Li T. S. et al., 2017, ApJ, 844, 74
López-Corredoira M., Cabrera-Lavers A., Garzón F., Hammersley P. L., 2002, A&A, 394, 883
Minchev I., Quillen A. C., Williams M., Freeman K. C., Nordhaus J., Siebert A., Bienaymé O., 2009, MNRAS, 396, L56
Monari G., Famaey B., Siebert A., Wegg C., Gerhard O., 2019, A&A, 626, A41
Moster B. P., Naab T., White S. D. M., 2013, MNRAS, 428, 3121
Myeong G. C., Vasiliev E., Iorio G., Evans N. W., Belokurov V., 2019, MNRAS, 488, 1235
Niederste-Ostholt M., Belokurov V., Evans N. W., Peñarrubia J., 2010, ApJ, 712, 516
Petersen M. S., Weinberg M. D., Katz N., 2019, preprint (arXiv:1903.08203)
Poggio E., Laporte C. F. P., Johnston K. V., D'Onghia E., Drimmel R., Grion Filho D., 2021, MNRAS, preprint (arXiv:2011.11642)
Poggio E., Drimmel R., Andrae R., Bailer-Jones C. A. L., Fouesneau M., Lattanzi M. G., Smart R. L., Spagna A., 2020b, Nat. Astron., 4, 590
Price-Whelan A. M., Johnston K. V., Sheffield A. A., Laporte C. F. P., Sesar B., 2015, MNRAS, 452, 676
Purcell C. W., Bullock J. S., Tollerud E. J., Rocha M., Chakrabarti S., 2011, Nature, 477, 301
Quillen A. C., 2003, AJ, 125, 785
Quillen A. C., Minchev I., 2005, AJ, 130, 576
Ramos P., Antoja T., Figueras F., 2018, A&A, 619, A72
Reylé C., Marshall D. J., Robin A. C., Schultheis M., 2009, A&A, 495, 819
Sawala T. et al., 2016, MNRAS, 456, 85
Sellwood J. A., Trick W. H., Carlberg R. G., Coronado J., Rix H.-W., 2019, MNRAS, 484, 3154
Sheffield A. A., Price-Whelan A. M., Tzanidakis A., Johnston K. V., Laporte C. F. P., Sesar B., 2018, ApJ, 854, 47
Skowron D. M. et al., 2019, Science, 365, 478
Toth G., Ostriker J. P., 1992, ApJ, 389, 5
Trick W. H., Coronado J., Rix H.-W., 2019, MNRAS, 484, 3291
Trick W. H., Fragkoudi F., Hunt J. A. S., Mackereth J. T., White S. D. M., 2021, MNRAS, 500, 2645
Vasiliev E., Belokurov V., 2020, MNRAS, 497, 4162

Velazquez H., White S. D. M., 1999, MNRAS, 304, 254
Vesperini E., Weinberg M. D., 2001, in Funes J. G., Corsini E. M., eds, ASP Conf. Ser. Vol. 230, Galaxy Disks and Disk Galaxies. Astron. Soc. Pac, San Francisco, p. 457
Walker I. R., Mihos J. C., Hernquist L., 1996, ApJ, 460, 121
Weinberg M. D., 1998, MNRAS, 299, 499
Weinberg M. D., 1999, in Gibson B. K., Axelrod R. S., Putman M. E., eds, ASP Conf. Ser. Vol. 165, The Third Stromlo Symposium: The Galactic Halo. Astron. Soc. Pac., San Francisco, p. 100
Weinberg M. D., Blitz L., 2006, ApJ, 641, L33
Weinberg M. D., Petersen M. S., 2021, MNRAS, 501, 5408
Widrow L. M., Gardner S., Yanny B., Dodelson S., Chen H.-Y., 2012, ApJ, 750, L41
Widrow L. M., Barber J., Chequers M. H., Cheng E., 2014, MNRAS, 440, 1971
Williams M. E. K. et al., 2013, MNRAS, 436, 101
Xu Y., Newberg H. J., Carlin J. L., Liu C., Deng L., Li J., Schönrich R., Yanny B., 2015, ApJ, 801, 105

APPENDIX A: SUMMARY PLOTS FOR DISC INFLUENCES

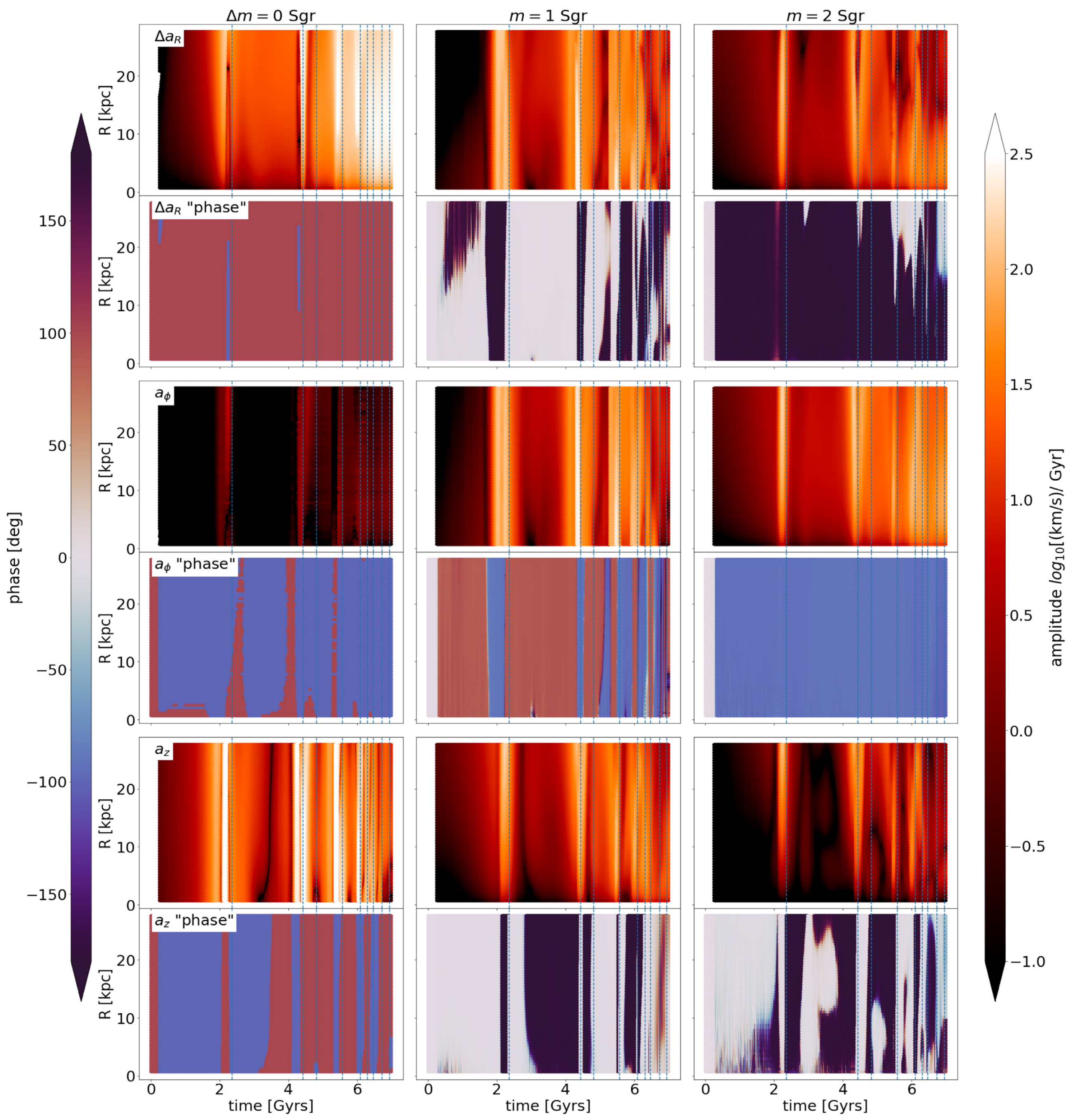

Figure A1. Amplitudes and phases for Sagittarius. Layout is the same as Figs 7 and A2.

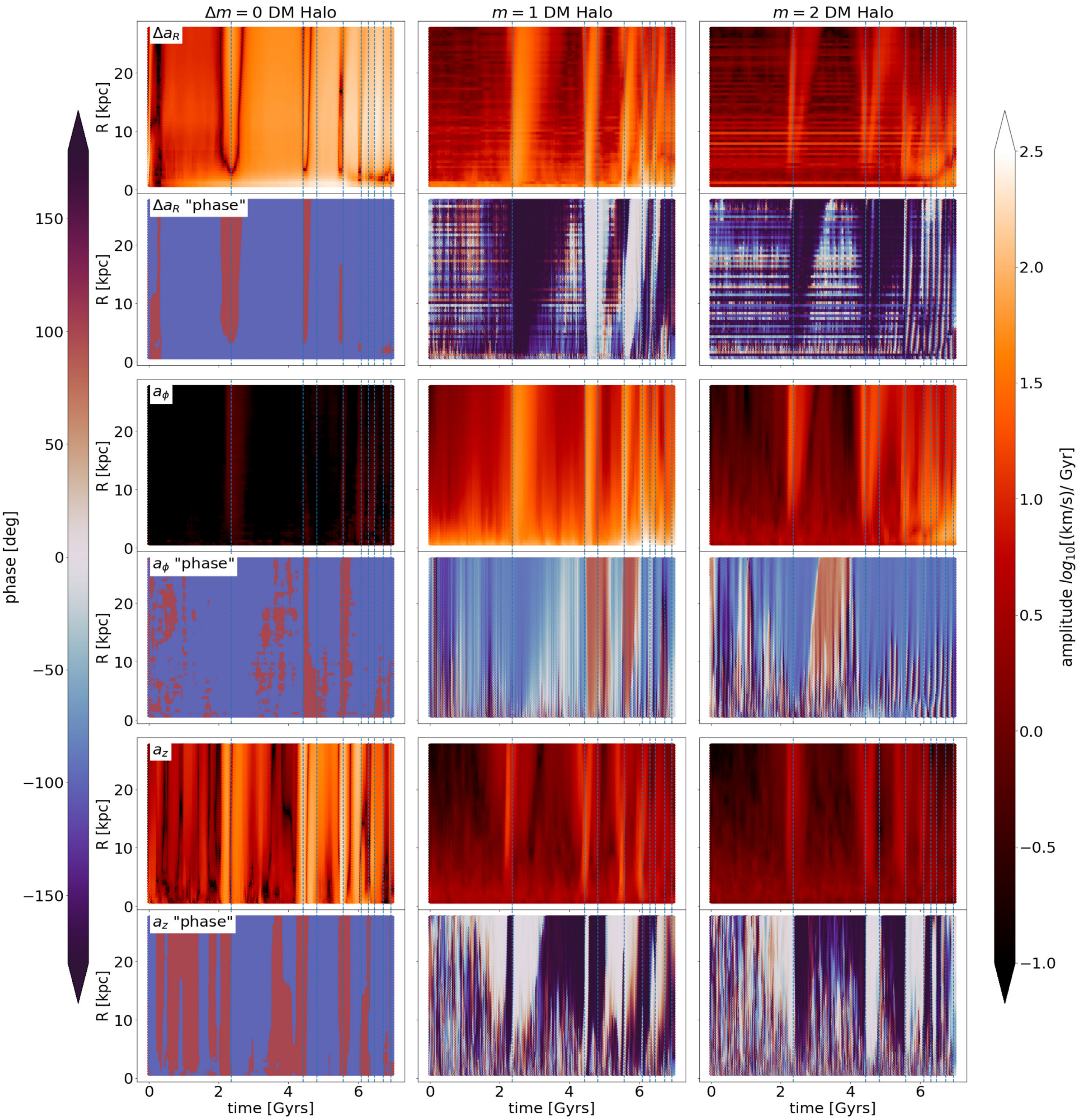

Figure A2. Amplitudes and phases for the dark matter halo. Layout is the same as Figs 7 and A1.

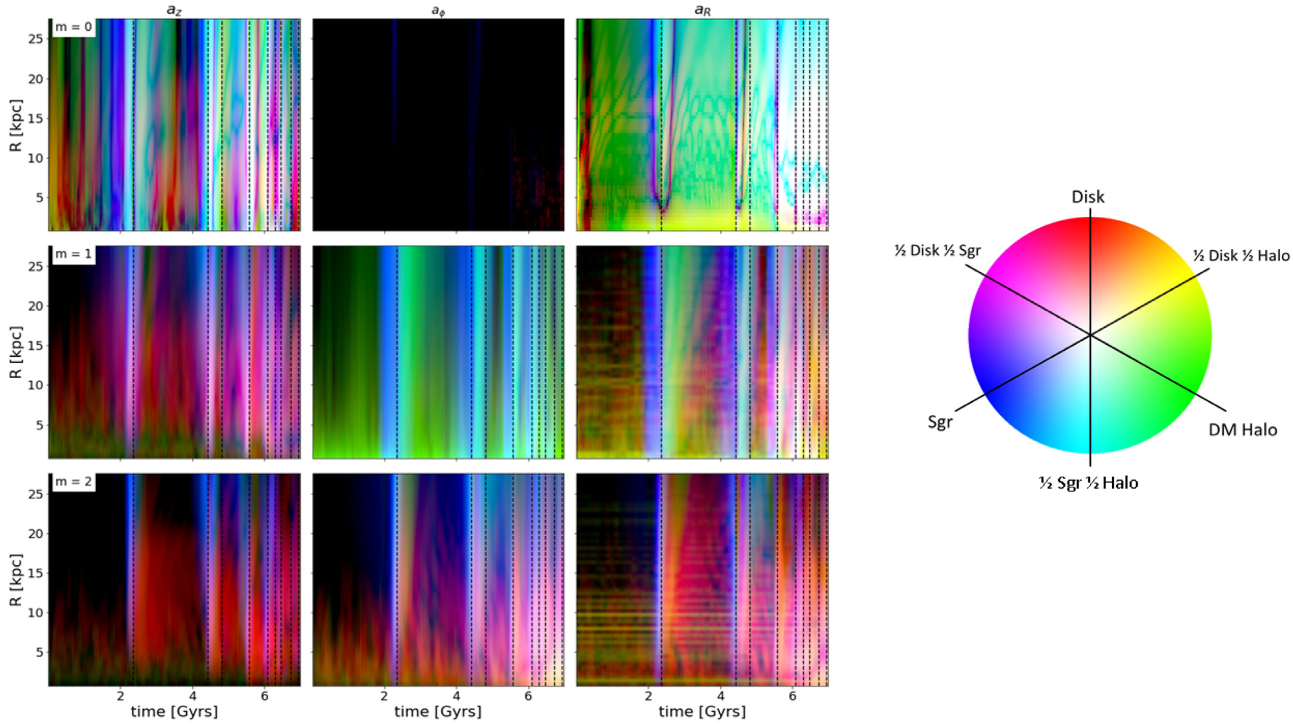

Figure A3. Fourier decomposition and comparison of the accelerations on the disc mid-plane due to each simulation component. Each panel shows the Fourier amplitude as a function of galactocentric radius R (y-axis) and time (x-axis) from all components. The columns are organized by acceleration, going from left to right with a_z, a_ϕ, and a_R. Rows are organized by ascending Fourier modes. For each Fourier mode and cylindrical acceleration, the component's respective influence on the disc is coloured separately and compared. The tidal influences from the DM Halo and Sgr are coloured in green and blue, respectively, while the disc self-gravity is coloured in red. Areas where more than one component have a large influence get a mix of these three colours. The higher the amplitude of a given component's influence, the more saturated the respective colour will be. As such, areas where all three components have high saturation, the combination of all colours will be close to white (an example of this is the right side of the top-right panel). On the other hand, low amplitudes reduces the saturation, meaning that darker regions have low influence (outer disc during the first Gyr in the bottom left panel). To the right of the figure is a colour wheel legend for how to interpret this mix of colours. An example of how a panel from this figure is assembled can be found in Fig. 8.

This paper has been typeset from a TEX/LATEX file prepared by the author.